NeuroImage: Clinical 9 (2015) 322–337

Contents lists available at ScienceDirect

NeuroImage: Clinical

journal homepage: www.elsevier.com/locate/ynicl

Regional vulnerability of longitudinal cortical association connectivity Associated with structural network topology alterations in preterm children with cerebral palsy

Rafael Ceschin[a,b], Vince K. Lee[a], Vince Schmithorst[a], Ashok Panigrahy[a,b,c,d,*]

[a] Department of Pediatric Radiology, Children's Hospital of Pittsburgh of UPMC, Pittsburgh, PA, USA
[b] Department of Biomedical Informatics, University of Pittsburgh School of Medicine, Pittsburgh, PA, USA
[c] Department of Radiology, Children's Hospital Los Angeles, Los Angeles, CA, USA
[d] Brain and Creativity Institution, University of Southern California, Los Angeles, CA, USA

ARTICLE INFO

Article history:
Received 1 July 2015
Received in revised form 5 August 2015
Accepted 24 August 2015
Available online 6 September 2015

Keywords:
Cerebral palsy
Periventricular leukomalacia
Diffusion tensor imaging
Probabilistic tractography
Visual cortical association fibers
Principal component analysis

ABSTRACT

Preterm born children with spastic diplegia type of cerebral palsy and white matter injury or periventricular leukomalacia (PVL), are known to have motor, visual and cognitive impairments. Most diffusion tensor imaging (DTI) studies performed in this group have demonstrated widespread abnormalities using averaged deterministic tractography and voxel-based DTI measurements. Little is known about structural network correlates of white matter topography and reorganization in preterm cerebral palsy, despite the availability of new therapies and the need for brain imaging biomarkers. Here, we combined novel post-processing methodology of probabilistic tractography data in this preterm cohort to improve spatial and regional delineation of longitudinal cortical association tract abnormalities using an along-tract approach, and compared these data to structural DTI cortical network topology analysis. DTI images were acquired on 16 preterm children with cerebral palsy (mean age 5.6 ± 4) and 75 healthy controls (mean age 5.7 ± 3.4). Despite mean tract analysis, Tract-Based Spatial Statistics (TBSS) and voxel-based morphometry (VBM) demonstrating diffusely reduced fractional anisotropy (FA) reduction in all white matter tracts, the along-tract analysis improved the detection of regional tract vulnerability. The along-tract map-structural network topology correlates revealed two associations: (1) reduced regional posterior–anterior gradient in FA of the longitudinal visual cortical association tracts (inferior fronto-occipital fasciculus, inferior longitudinal fasciculus, optic radiation, posterior thalamic radiation) correlated with reduced posterior–anterior gradient of intra-regional (nodal efficiency) metrics with relative sparing of frontal and temporal regions; and (2) reduced regional FA within frontal–thalamic–striatal white matter pathways (anterior limb/anterior thalamic radiation, superior longitudinal fasciculus and cortical spinal tract) correlated with alteration in eigenvector centrality, clustering coefficient (inter-regional) and participation co-efficient (inter-modular) alterations of frontal–striatal and fronto-limbic nodes suggesting re-organization of these pathways. Both along tract and structural topology network measurements correlated strongly with motor and visual clinical outcome scores. This study shows the value of combining along-tract analysis and structural network topology in depicting not only selective parietal occipital regional vulnerability but also reorganization of frontal–striatal and frontal–limbic pathways in preterm children with cerebral palsy. These finding also support the concept that widespread, but selective posterior–anterior neural network connectivity alterations in preterm children with cerebral palsy likely contribute to the pathogenesis of neurosensory and cognitive impairment in this group.

1. Introduction

One of the most common types of cerebral palsy is spastic diplegia, which is thought to be related to perinatal preterm white matter injury or periventricular leukomalacia (PVL). The topography of the neuropathology of PVL includes both a focal and diffuse component, with regional vulnerability of the parietal–occipital white matter and crossing fibers of the deep cerebral white matter. In conjunction with these motor abnormalities, these patients are also known to have a host of neurocognitive problems including visual-motor and visual perception disabilities, which are associated with various types of frontal executive-attention deficits. The distribution of the neural network substrate that underlies this neurocognitive phenotypic disability is poorly

* Corresponding author at: Department of Pediatric Radiology, Children's Hospital of Pittsburgh of UPMC, Pittsburgh, PA, USA. Tel.: +1 412 692 5510 (Secretary); fax: +1 412 692 6929.
E-mail address: panigrahya@upmc.edu (A. Panigrahy).

http://dx.doi.org/10.1016/j.nicl.2015.08.021

understood and is likely related to regional vulnerability of cortical association pathways and compensatory brain reorganization.

Diffusion weighted imaging techniques, including Diffusion Tensor Imaging (DTI) and diffusion tensor tractography (DTT), can be used for the detection of white matter microstructural changes (Mori and Zhang, 2006; Gerig et al., 2004) that likely underlie the disability associated with cerebral palsy. In the last several years, numerous groups have reported DTI-based white matter differences in this population. The majority of studies have predominately focused on regions of the brain associated with putative sensorimotor function and demonstrate variable deficits (Scheck et al., 2012; Hoon et al., 2002; Murakami et al., 2008; Ludeman et al., 2008; Chang et al., 2012; Trivedi et al., 2010; Rose et al., 2007) (for systematic review see Scheck et al., 2012). For the most part, these studies use similar approaches and typically measure diffusivity and anisotropy within a priori selected white matter (WM) regions of interest (ROIs) related to sensorimotor function. Additional studies utilizing deterministic based tractography methods, mainly Fiber Assignment by Continuous Tracking (FACT), are likewise focused on the identification of a priori sensorimotor tracts as ROIs for quantification of diffusivity measurements (Rose et al., 2011; Thomas et al., 2005; Yoshida et al., 2010; Rha et al., 2012). More recently there have been descriptive reports of structural network topology alterations in children with cerebral palsy. However, there is relatively less information about correlating regional vulnerability of longitudinal cortical association tracts with structural network topology changes in this population.

There are a few DTI studies investigating more global WM deficits, also demonstrating changes in mean diffusivity and fractional anisotropy measures in children with CP (Rai et al., 2013; Lee et al., 2011). In a tractography study, Nagae et al. found multiple and wide-spread differences in a qualitative assessment of 26 manually defined fiber tracts (Nagae et al., 2007). These studies suggest a more diffuse pattern of white matter injury, and indicate the need for a more comprehensive whole brain characterization of white matter damage in CP. The technique of DTI has been used to study both cortical spinal tract and cortical association white matter in survivors of prematurity with cerebral palsy (Nagae et al., 2007; Pandit et al., 2013; Hoon et al., 2009; Counsell et al., 2007), but these studies have typically relied only on tractography post-processing methods based on the FACT algorithm. These more traditional tractography methods typically collapse each tract's diffusion data into a single numeric mean average, resulting in loss of visualization and analysis of regional variation in diffusion metrics along the tracts. Diffusion measurements can vary along the course of a tract for multiple reasons. First, certain axons within a fascicle of a white matter tract do not necessarily follow the course of the entire tract, as groups of axons arising of a common neuronal cell group may enter the white matter fascicle at one point and then eventually exit the same fascicle at a different point. Second, there is regional decrease in fractional anisotropy in areas of crossing fibers, in which a segment of most of the longitudinal cortical association fibers in the brain will travel through. Third, both normal developmental processes and pathological conditions have been recently shown to have regional tract variation using different types of along the tract trajectory analysis. Combining more refined tractography analysis with structural topology analysis may help us understand how regional vulnerability of specific cortical association tracts can be interrelated to more global dynamics in the alteration of neural networks that can underlie the more complex neurocognitive phenotypes observed in these patients.

In this study, we tested the hypothesis that there would be selective regional vulnerability of cortical association tracts in preterm children with PVL that would correlate with structural network topology differences. We first delineate the degree of diffuse microstructural abnormalities using both standard averaged measurements from probabilistic tractography data, Tract-Based Spatial Statistics (TBSS) and template based voxel-based morphometry (VBM) analysis. We then delineated regional cortical association longitudinal tract variation using probabilistic tractography and along tract analysis, supplemented by population distribution maps. We targeted our primary tractography analysis to study cortical association longitudinal fiber tract including the inferior longitudinal fasciculus (ILF) and the inferior fronto-occipital fasciculus (IFOF) (intrahemispheric pathways and ventral visual stream correlates), superior longitudinal fasciculus (intrahemisperic pathway with integration of visual pathways with the posterior frontal regions), the posterior thalamic radiations (cortical thalamic including connection from pulvinar to the parietal cortex), the anterior thalamic radiation (including both frontal–thalamic and frontal–striatal pathways) and the optic radiation (primary visual relay). Next, we calculated structural network topology measurements in this same preterm cerebral palsy cohort and compared to a healthy control group, to determine if there was any compensatory regional reorganization that was associated with regional vulnerability of the longitudinal cortical association fiber tracts. Lastly, we correlated both along tract and global structural network topology measurements with motor and visual outcome measurements.

2. Methods

2.1. Subjects

The cohorts analyzed in this study have been previously described (Nagasunder et al., 2011). The inclusion criteria for the preterm survivors with cerebral palsy were: 1) prematurity (<37 gestational weeks at birth); 2) confirmed cerebral palsy by medical history and neurological examination; and 3) evidence for the sequelae of periventricular leukomalacia on conventional MRI performed during childhood. These sequelae were defined as periventricular volume loss and signal hyperintensities on FLAIR as previously described (Nagasunder et al., 2011; Panigrahy et al., 2001). Additionally, preterm children with retinopathy of prematurity were excluded from our study as a subset of these preterm children was originally recruited as part of a neonatal visual functional MRI study (Ceschin et al., 2015). The controls were children born at term (37–42 gestational weeks) with normal conventional MRI performed in the same age range in childhood as the preterm cohort.

Written consents for use of their child's clinically acquired MRI data and for participation in additional neurodevelopmental and neuroimaging studies were obtained from parents on behalf of the prospectively recruited patients by a research coordinator. The ethics committee approved this consent process. Additionally, as this study involved a retrospective review of all clinically-acquired neuroimaging data for the period between 2005 and 2009, which included subjects who were not enrolled into prospective studies, approval was also obtained for the retrospective use of all clinically acquired MRI data obtained between 2005 and 2009.

2.2. MRI procedures and analysis

2.2.1. Image acquisition and pre-processing

Imaging was acquired on a 1.5 T General Electric System (Ge-Medical Systems, Milwaukee, WI) using a pediatric head coil. Diffusion tensor images were acquired using the following parameters: echo-planar imaging (EPI) sequence, TE/TR = 80/10,000 ms, field of view = 22 cm, matrix = 128 × 128, in-plane resolution of 2.5 mm, 25 directions and b-value of 1000 s/mm^2.

Standard pre-processing steps were performed using routines in FSL. Subject DTI images were motion and eddy current corrected using a rigid body registration, followed by brain extraction using Brain Extraction Tool (BET). DTI metrics, including fractional anisotropy (FA), signal intensity without diffusion weighting (S0), value of the principal eigenvalue (L1), and direction of the principal eigenvector were computed for each voxel.

2.2.2. TBSS and template based VBM-like voxelwise analyses

In order to investigate regional differences in FA, we used both TBSS analysis and a template based VBM analysis. TBSS data analysis was performed using Oxford University's FMRIB FSL software (Version 4.1.4) (Jenkinson et al., 2012). Our protocol for TBSS (Paquette et al., 2013) was similar to other published methods previously optimized for the infants. All registration steps were visually inspected for registration errors in order to minimize any noise due to white matter loss or poor image quality. Subjects were excluded if we were unable to attain suitable registration to the template image. Voxelwise statistics (Student's T-test between CP and controls) were performed using Threshold-Free Cluster Enhancement (TFCE) to correct for multiple comparisons and thresholded at corrected $p < 0.05$.

As an alternative to TBSS, which may possibly be vulnerable to spurious findings caused by morphological differences, we also performed a template-based voxel-based morphometry (VBM)-like analysis. Our VBM-like analysis was done by first normalizing the subject's L1 images to an EPI template in MNI space using SPM8. Then, the L1 images were averaged together and coregistered to the EPI template in order to generate a study-specific template. The original L1 images were then normalized to this newly generated template, and the resulting transformations were applied to each subject's corresponding FA images. The brains were segmented into gray matter, white matter, and CSF using the multi-modal segmentation routine in SPM8 using the FA and S0 images as inputs (this procedure was found to produce more robust segmentation of white matter). Only voxels in white matter (WM probability >0.9) were included in subsequent analyses, ensuring that our VBM analysis was robust to possible spurious findings due to image misregistration. Voxelwise statistics (Student's T-test between CP and controls) were performed; T-scores were spatially filtered with $\sigma = 3$ mm. Monte Carlo analysis (Ledberg et al., 2001) was used in order to find intensity and spatial extent thresholds corresponding to a FWE-corrected $p < 0.05$.

2.2.3. Along-tract analysis

Traditionally, tractography methods have looked at diffusivity metrics averaged across the entire span of the delineated tract. These methods are insensitive to local tract variability, particularly in long cortico-cortical connections. We aimed to introduce a local anatomical dimension to probabilistic tractography analysis. The pipeline for the along-track analysis involves a number of steps, described in order below.

2.2.3.1. Probabilistic tractography. Probabilistic estimation of diffusion parameters was performed using the BedpostX procedure included in FSL. Probabilistic tractography takes a different approach to fiber tracking than traditional deterministic algorithms. Where conventional algorithms assume that each voxel contains a single fiber direction modeled in a winner-takes-all function, probabilistic tracking aims to model two (or more) probable directions at each voxel. Diffusion parameters are estimated using Markov Chain Monte Carlo, and tracking is done by repeatedly sampling streams originating from each voxel in the user defined seed mask along the diffusion distribution previously generated. The result is a probability map of the tract's estimated path given the seed mask and optional waypoint and exclusion masks. A probabilistic model allows for a more robust tracking framework, enhancing tract resolution, especially along regions of crossing fibers and low signal (Behrens et al., 2007). This is a particularly desirable feature in injured cohorts where FA in the tract of interest may drop below the detectable threshold set by deterministic models, as well as neonatal populations where a naturally low FA exists due to unmyelinated white matter. In spite of this increased sensitivity, probabilistic tractography is still subject to noise and distortion. To attenuate these effects, the raw probability maps can be thresholded at a desirable confidence level which reliably delineates anatomically sound tracts while reducing extraneous paths. This approach is analogous to "tract refining" or "tract pruning" methods employed in deterministic models.

2.2.3.2. Quantification. The large age range in our population presents the issue of varying brain volumes and subsequent ROI size. White matter loss in the CP cohort is a further confound. To account for this, extracted tracts were normalized by conservatively thresholding to only include voxels that receive a total number of streamlines equivalent to at least 1% of the waytotal (i.e., 1% of streamlines that successfully traversed the corresponding waypoint mask). These thresholded tracts were then binarized and overlaid onto the diffusivity maps of interest in order to acquire mean values along the span of the tracts. Paired t-tests were performed between bilateral tracts, thresholded at $p < 0.01$, in order to test for asymmetry. Tracts with no significant contralateral difference were averaged for all subsequent comparative whole-tract analyses.

2.2.3.3. Tracts. Our tracts of interest were bilateral corticospinal tract (CST) as a motor control, bilateral anterior (ATR) and posterior thalamic radiations (PTR), bilateral optic radiations (OR), bilateral inferior fronto-occipital fasciculus (IFOF) and bilateral inferior longitudinal fasciculus (ILF). Tracts were delineated following the Catani and Thiebaut de Schotten (2008) reference atlas. The atlas provides standard and practical reference to delineate tracts using large, robust seed and waypoint masks in order to minimize tract variability derived from potentially variable mask placement. All masks were manually drawn in each subject's diffusion space.

Corticospinal tracts were delineated by using FA color maps as reference and placing seed ROI at the level of the cerebral peduncle with waypoint ROI at the corresponding posterior limb of the internal capsule and an exclusion mask at the midline. Thalamic radiations were delineated by defining the seed masks as the whole right or left thalamus at one axial slice at the level of the splenium of the corpus callosum. Anterior thalamic radiation was generated by placing the waypoint mask at one entire coronal plane one slice anterior to the genu of the corpus callosum and exclusion mask at the sagittal midline. Posterior thalamic radiation was generated by placing waypoint mask at one entire coronal plane one slice posterior to the splenium of the corpus callosum and exclusion mask at the sagittal midline. Optic radiations were seeded as the lateral geniculate nucleus, with the same waypoint and exclusion as the PTR. ILF and IFOF tracts were seeded as the entire volume of anterior–posterior directional white matter in the occipital lobe. A single waypoint for the ILF was the volume of white matter in the temporal lobe, while the IFOF used one waypoint as the entire external/extreme capsule and one coronal plane one voxel anterior to the genu of the corpus callosum. OR, ILF, and IFOF tracking included a mid-line exclusion mask.

2.2.3.4. Registration. A different registration approach was used for the along-track analysis as compared to the VBM-like voxelwise analysis. Each subject's fractional anisotropy maps were first linearly registered to FMRIB58 FA standard space using FSL's FLIRT linear registrations tool using a 12 degree of freedom affine transformation. The resulting transformation matrices were applied to the subject's corresponding binarized delineated tracts. The linearly transformed FA images were then used as the input to non-linearly register each subject's image into FMRIB58 FA standard space using FSL's FNIRT non-linear registration tool, using a bending energy regularization model and global linear intensity mapping. The resulting warps were applied to the corresponding, previously transformed tracts. All registered images were visually inspected for accurate registration, and erroneous subjects were excluded from the subsequent analyses.

2.2.3.5. Spatial distribution. In order to purely compare general tract distribution among the cohorts, right and left spatially normalized tracts were averaged on each population by flipping the left side tracts over

the mid-sagittal plane and averaging with their contralateral counterparts. The spatial distribution maps were generated by overlaying each cohort's averaged bilateral tracts onto standard space and thresholding to only include voxels containing at least 10% of all subject tracts. Fig. 1A shows an example spatial distribution map comparing the corticospinal tract (CST) between controls and PVL groups. This map gives a visual representation of each tract's anatomical variability within each population using a standard space reference point.

2.2.3.6. Statistical analysis. The mean FA value of each tract, for each subject warped into standard space, was taken at every slice along the principal longitudinal direction of each fiber of interest. The non-linearly warped tracts and relatively low variability in tract profiles across subjects gives us confidence in the local anatomical correlate across individuals. This method works well with long cortical fibers, but loses its informative value at tract curvatures, notably at callosal fibers (not delineated in this study). Fig. 1B shows the tract profiles for the right CST

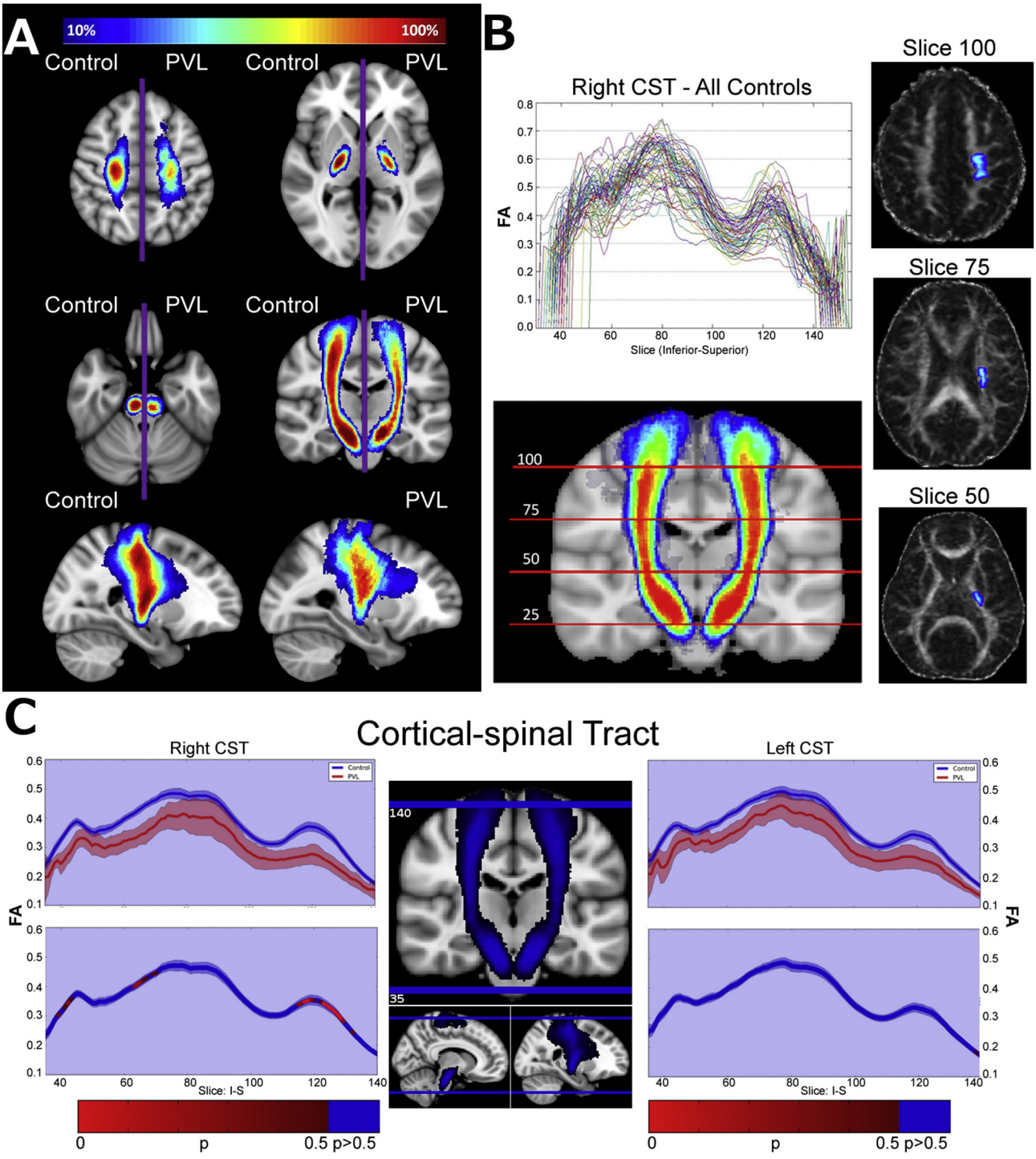

Fig. 1. Diagram of spatial distribution map technique/along tract analysis methodology using the cortical spinal tract. A) Comparison of spatial distribution of corticospinal tract (CST) after normalization to MNI space, between control and PVL groups. B) Example tract profile generation using the right CST for all controls. Valleys correspond to known regions of crossing fibers. C) Statistical comparison of bilateral tract profiles between control (blue) and PVL (red) groups. Along-tract statistics were performed using the Welch t-test and family-wise error was controlled for by permutation test.

delineated from all control subjects. The observed "valleys" correspond to regions of crossing fibers where a drop in FA is expected.

Mean estimators were bootstrapped to attenuate the variance caused by the low sample of the injured cohort, and the 95% confidence intervals (CI) of the distribution were used for visualization (Fig. 1C). Statistical analysis was performed using Welch t-test due to unequal between-cohort variance. Family-wise error was controlled for by permuting group labels across each tract over several iterations, thus building up a null distribution across the entire tract using a step-down Westfall and Young permutation algorithm. The newly formed null distribution was used to determine the significance level at each point along the tract using permutation tests at each individual slice.

2.2.4. Structural network topology (graph analysis)

2.2.4.1. Pre-processing. Deterministic tractography was performed using in-house software written in IDL (http://www.ittvis.com, Boulder, CO). Streamlines were computed from each voxel with FA > 0.25 in both directions. Stopping thresholds for the tractography were: turning angle >45° or FA < 0.25.

The DTI data were segmented into 76 anatomical regions by applying the automated anatomic labeling (AAL) template (Tzourio-Mazoyer et al., 2002). The AAL parcellation atlas was normalized into each subject's native space by applying the reverse of the transformation found for the template based VBM-like analysis. This procedure obtains the greater between-participant accuracy obtainable via a study-specific template, while also ensuring that the template corresponds to MNI space. The anatomical scans were without gross anatomical abnormalities which could conceivably impact the spatial transformations (Rivkin et al., 2013) and all transformations were verified via visual inspection.

Each of the 76 regions in the parcellation atlas served as a node in the subsequent topological analyses. 76-×-76 adjacency matrices were constructed for each subject, with each non-diagonal element containing one if there was at least one streamline connecting the two regions, and zero if not.

2.2.4.2. Graph metrics and statistical analysis. Global graph metrics (cost, global efficiency, assortativity, and modularity) were computed via the C++ modules available from the Brain Connectivity Toolbox (BCT; Indiana University) and in-house routines in IDL; nodal metrics (nodal efficiency, eigenvector centrality, participation coefficient, and clustering coefficient) were also computed. (For further details, see the BCT documentation at https://sites.google.com/site/bctnet/ (Rubinov and Sporns, 2010).) Metrics were compared between groups using a Student's T-test.

2.2.4.3. Graph visualization details. For visualization purposes, the spring-loading technique (Fruchterman and Reingold, 1991) was used: graphs were modeled with each node as a positively-charged particle (repelling each other) but connected via springs, with spring constants equal to the connection strength. This procedure results in more strongly-connected nodes appearing closer together in the graph. The visualizations were color-coded according to the specific modules to which each node belonged, with intra-modular connections drawn as a specific color (red, orange, cyan, or green) and inter-modular connections drawn as black. Circle connectivity plots were generated using Circos (Krzywinski et al., 2009). Anatomical regions were segmented and grouped using existing AAL template labels, with groups arranged by hemisphere and physical anatomical location.

2.3. Clinical neuromotor and visual outcome scores

Individuals were classified using the Gross Motor Function Classification System (GMFCS) score and all cases were classified into a severe group (GMFCS of IV, n = 9), and a moderate group (GMFCS of II or III, n = 8). The moderate and severe group distinction used here separates the participants according to their level of self-mobility. According to the GMFCS criteria, individuals in levels II or III are able to walk with assistance from a hand held mobility device after age 4, however individuals classified as level IV have more limited self-mobility, and are more likely to be transported in a manual or powered wheelchair. GMFCS assessment can be performed on children prior to age 4 and is predictive and reliable of functional abilities throughout development (Palisano et al., 1997, 2007). Opthalmological examinations were also performed and rated as normal or abnormal based upon visual acuity and visual-motor examination.

2.3.1. Statistical analyses

We wished to relate structural measures from network topology and along-tract analysis to the neuromotor and visual scores. For the correlation of structural network global measures and clinical motor and visual outcome scores, we used simple linear regression analysis. For the along-tract analyses, however, we wished to estimate their predictive value. Due to the small sample size of the training dataset of the along tract dataset (16 abnormal subjects, after exclusions due to poor image quality), we first used a bootstrapping method to generate a new dataset containing 1000 preterm cerebral palsy cases and 1000 term controls by sampling with replacement from the original datasets. This helps attenuate any large outlier influences and lowers the sample variance. To reduce the dimensionality of the effects and control for the inherent dependence of sequential along-tract measurements, we used principal component analysis (PCA) to reduce the newly generated dataset into orthogonal components accounting for at least 80% of the variance in each tract of interest. Finally, we used the extracted components as covariates in a logistic regression, with additional covariates post-conceptional age (PCA) and gestational age (GA). We used the area under the ROC (AUROC) as a measure of the predictive power of each given model.

3. Results

3.1. Clinical database and conventional MR findings

The volumetric study included 17 preterm PVL patients (post-conceptional age [PCA] mean ± SD: 5.6 ± 4 years; range: 1.0–14.3 years) and 74 controls (5.7 ± 3.4 years; range: 1.8–12.7 years). The PVL patients were born at 24–36 gestational weeks and were similar in PCA to the control group (p = 0.90). Of these subjects, a subset of 16 PVL patients (5.7 ± 4.1 years; range: 1.0–14.3 years) and 68 controls (6.0 ± 3.4 years; range: 1.8–12.7 years) had DTI assessments due to the necessity of excluding DTI data in certain children with artifactual movement during imaging. As per study inclusion criteria, all of the PVL cases had cerebral white matter damage on conventional MRI. The T2/FLAIR signal hyperintensities in the PVL cases were both focal and confluent, and were found in the parieto-occipital white matter and region of the optic radiations in 100% of the cases. None of the PVL cases demonstrated focal T2/FLAIR hyperintensities in the deep frontal white matter or the temporal regions. The conventional imaging and clinical characteristic of this cohort have been previously described in detail (Nagasunder et al., 2011).

3.2. Standard tract-averaged probabilistic tractography analysis

Table 1 shows the summary diffusivity metrics for all delineated tracts. Significant differences in averaged tract values were detected between the preterm PVL cases and controls in all of the visual cortical association tracts examined. In all three cortical thalamic tracts, the preterm PVL cases demonstrates reduced fractional anisotropy ranging from 15–25% with different degrees of diffusivity abnormality. The ATR demonstrates relatively normal diffusivity values, while the optic

Table 1
Probabilistic tractography averaged diffusivity metrics.

Tract	Metric	Control		PVL		pval
		Mean	SD	Mean	SD	
ATR	FA	0.3000	0.0443	0.2300	0.0779	0.0042
	RD	0.0007	0.0001	0.0007	0.0002	0.7832
	MD	0.0009	0.0001	0.0008	0.0003	0.9008
	AD	0.0011	0.0001	0.0011	0.0003	0.4944
CST	FA	0.4020	0.0528	0.3410	0.0472	0.0001
	RD	0.0006	0.0001	0.0008	0.0001	0.0003
	MD	0.0008	0.0001	0.0010	0.0001	0.0004
	AD	0.0012	0.0001	0.0013	0.0001	0.0015
Genu	FA	0.4619	0.0647	0.3622	0.0821	0.0002
	RD	0.0007	0.0001	0.0009	0.0002	0.0026
	MD	0.0009	0.0001	0.0011	0.0002	0.0062
	AD	0.0014	0.0001	0.0015	0.0002	0.0749
IFOF	FA	0.3557	0.0497	0.2890	0.0555	0.0004
	RD	0.0007	0.0001	0.0009	0.0001	0.0011
	MD	0.0009	0.0001	0.0010	0.0001	0.0015
	AD	0.0012	0.0001	0.0013	0.0001	0.0071
ILF	FA	0.3161	0.0430	0.2551	0.0495	0.0003
	RD	0.0008	0.0001	0.0009	0.0001	0.0001
	MD	0.0009	0.0001	0.0011	0.0001	0.0001
	AD	0.0012	0.0001	0.0014	0.0001	0.0005
OR	FA	0.3559	0.0467	0.2800	0.0552	0.0001
	RD	0.0007	0.0001	0.0009	0.0002	0.0010
	MD	0.0009	0.0001	0.0011	0.0002	0.0016
	AD	0.0012	0.0001	0.0014	0.0002	0.0058
PTR	FA	0.3013	0.0324	0.2586	0.0512	0.0066
	RD	0.0007	0.0001	0.0009	0.0002	0.0014
	MD	0.0009	0.0001	0.0011	0.0002	0.0015
	AD	0.0011	0.0001	0.0014	0.0002	0.0020
SLF	FA	0.3194	0.0460	0.2379	0.0817	0.0018
	RD	0.0007	0.0001	0.0008	0.0002	0.0861
	MD	0.0008	0.0001	0.0009	0.0002	0.0471
	AD	0.0011	0.0001	0.0011	0.0002	0.2145
Splenum	FA	0.5047	0.0565	0.3390	0.1073	0.0000
	RD	0.0007	0.0001	0.0011	0.0005	0.0029
	MD	0.0010	0.0001	0.0014	0.0005	0.0068
	AD	0.0016	0.0001	0.0019	0.0005	0.0500

$p < 0.01$.
$p < 0.001$.

radiations and the PTR demonstrate reduced diffusivity. In all three intrahemispheric long range tracts (SLF, IFOF, ILF), there was also a reduction of fractional anisotropy which was associated with abnormal diffusivity. In contrast, the CST showed the smallest reduction in FA relative to most other cortical association tracts.

3.3. Diffuse microstructural abnormalities determined by TBSS and template-based VBM

The VBM maps of the preterm children with PVL were concordant with the TBSS results, showing diffuse decreased diffusivity in white matter throughout (Fig. 1). Compared to the controls, the preterm children with PVL were found to have significantly reduced fractional anisotropy (FA) in large sectors of the central and posterior white matter, bilaterally, extending into the midbrain and brainstem (Fig. 2). This included key regions within the visual system (i.e., posterior temporal–occipital white matter in region of the optic radiations, the inferior frontal–occipital fasciculus (IFOF), inferior longitudinal fasciculus, and the splenium of the corpus callosum), the limbic system (i.e., cingulum, fimbria, fornix) and the motor system (i.e., corona radiata, body of the corpus callosum, posterior limb of the internal capsule, crus pedunculi, middle cerebellar peduncles, and inferior cerebellar peduncles). Significant reductions in FA were also seen in frontal regions (either the deep white matter of the frontal lobe or in the region of the crossing of those fibers — the genu of the corpus callosum). However, when examining the regions that contained longitudinal visual association fibers, including the ILF, IFOF and the SLF, there was no clear regional FA abnormality noted.

3.4. Along-tract analysis of cortical association tracts

3.4.1. Inferior frontal–occipital fasciculus (IFOF)

In the controls, there were three distinct segments of the IFOF identified within the fractional anisotropy tract profile (Fig. 3) which corresponded to the trajectory of the fiber tract extending from the occipital/temporal lobe (Segment 1), coursing through the external capsule (Segment 2), towards the inferior frontal lobe (Segmental 3). The highest peak of FA values was in in the occipital–temporal segmental and the lowest peak of FA values was in the external capsule segment.

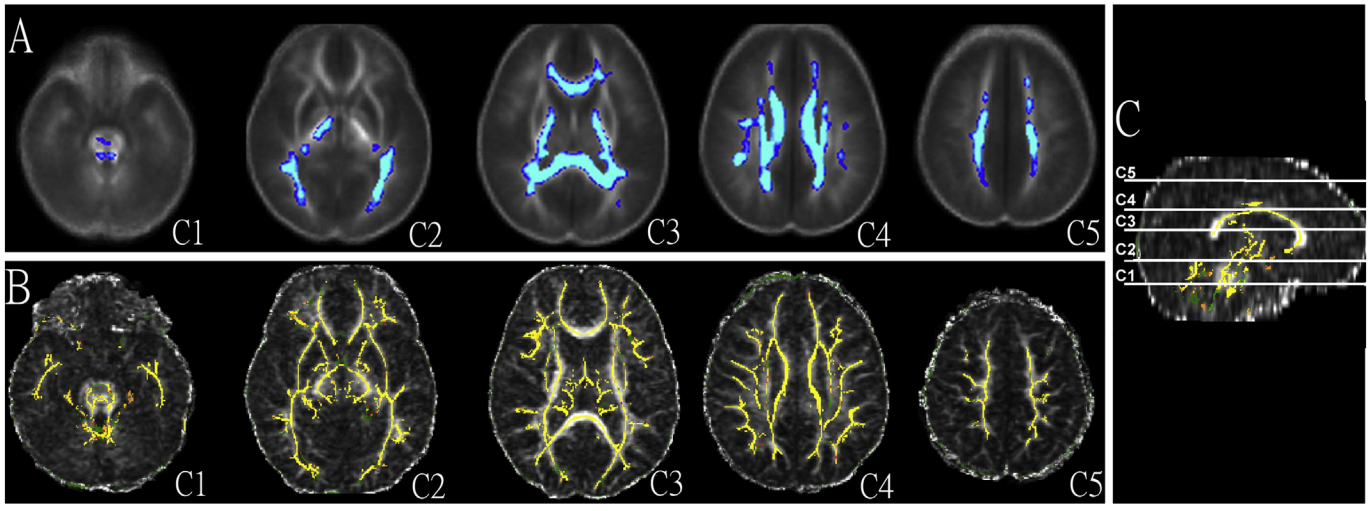

Fig. 2. Microstructural abnormalities determined by template based VBM (A) and TBSS (B). Compared to the controls, the preterm children with PVL were found to have significantly reduced fractional anisotropy (FA) in large sectors of the central and posterior white matter, bilaterally, extending into the midbrain and brainstem. This included key regions within the visual system (i.e., posterior temporal–occipital white matter in region of the optic radiations, the inferior frontal–occipital fasciculus (IFOF), inferior longitudinal fasciculus, and the splenium of the corpus callosum), the limbic system (i.e., cingulum, fimbria, fornix) and the motor system (i.e., corona radiata, body of the corpus callosum, posterior limb of the internal capsule, crus pedunculi, middle cerebellar peduncles, and inferior cerebellar peduncles). Significant reductions in FA were also seen in frontal regions (either the deep white matter of the frontal lobe or in the region of the crossing of those fibers — the genu of the corpus callosum). When examining the regions of that contained longitudinal visual association fibers tract, including the ILF, IFOF and the SLF, there was no clear regional FA abnormality noted that was comparable to the along tract and spatial distribution analysis.

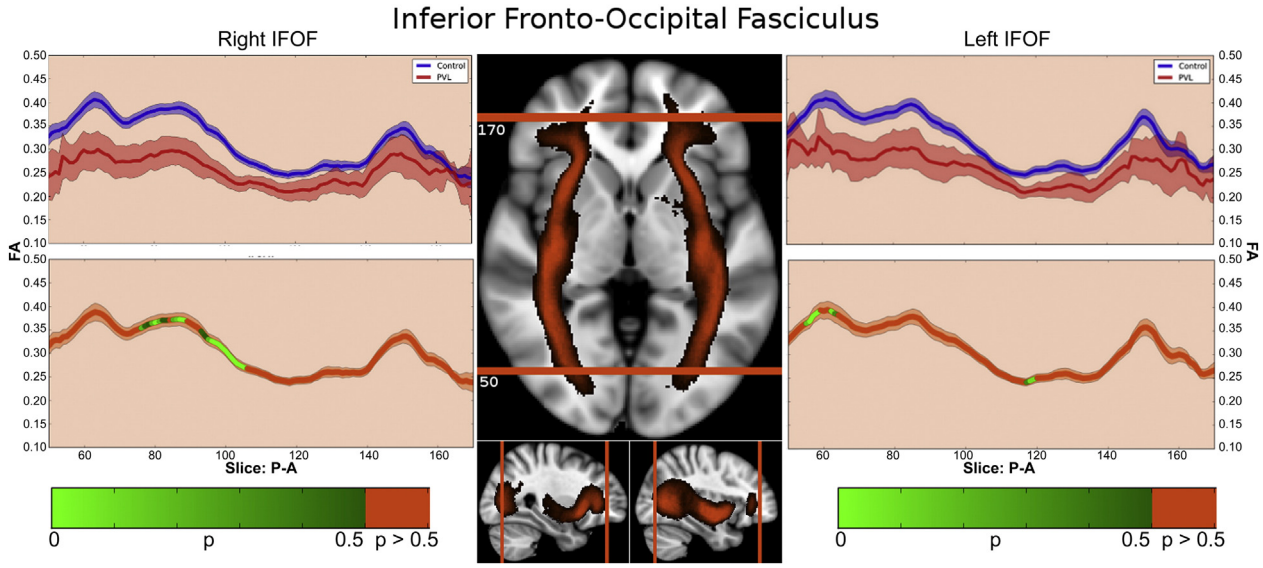

Fig. 3. Inferior frontal–occipital fasciculus (IFOF) along-tract statistics. In the controls, there were three segmental identified of the IFOF within the fractional anisotropy tract profile which corresponded to the trajectory of the fiber tract extending from the occipital/ temporal lobe (Segment 1), coursing through the external capsule (Segment 2), towards the inferior frontal lobe (Segmental 3). When comparing this FA tract profiles to the preterm PVL cases, the greatest reduction in FA occurred in Segment 1 and Segment 2, with a greater reduction noted within the occipital portion of the tract.

There was a small distinct peak in FA values in the region where the uncinate fasiculus joins with the IFOF and a relatively higher peak adjacent to the areas of the cross fibers within inferior frontal lobes. When comparing this FA tract profiles to the preterm PVL cases, the greatest reduction in FA occurred in Segment 1 and Segment 2, with a greater reduction noted within the occipital portion of the tract. The right and left IFOF did show similar distribution of both normal FA variance along the tract in the controls and the pattern of regional FA reduction in the preterm PVL cases, demonstrating no evidence of lateralization. The probabilistic spatial distribution maps did confirm both the anatomic and pathological regional variations (described above) of the IFOF in both the controls and preterm PVL cases (Supplementary Fig. 1).

3.4.2. Inferior longitudinal fasciculus (ILF)

There were two segments identified of the ILF within the fractional anisotropy tract profile (Fig. 4) which corresponded to the trajectory of the fiber tract extending from the occipital lobe to the temporal lobe, identified in the control population tract profile. The more posterior occipital segment demonstrated overall higher levels of fractional anisotropy compared to the more anterior temporal lobe segment. No distinct "peaks" were observed. When comparing this FA tract profiles to the preterm PVL cases, the greatest reduction in FA occurred in posterior occipital segment of the tract. The right and left ILF did show similar distribution of both normal FA variance along the tract in the controls and the pattern of regional FA reduction in the preterm PVL

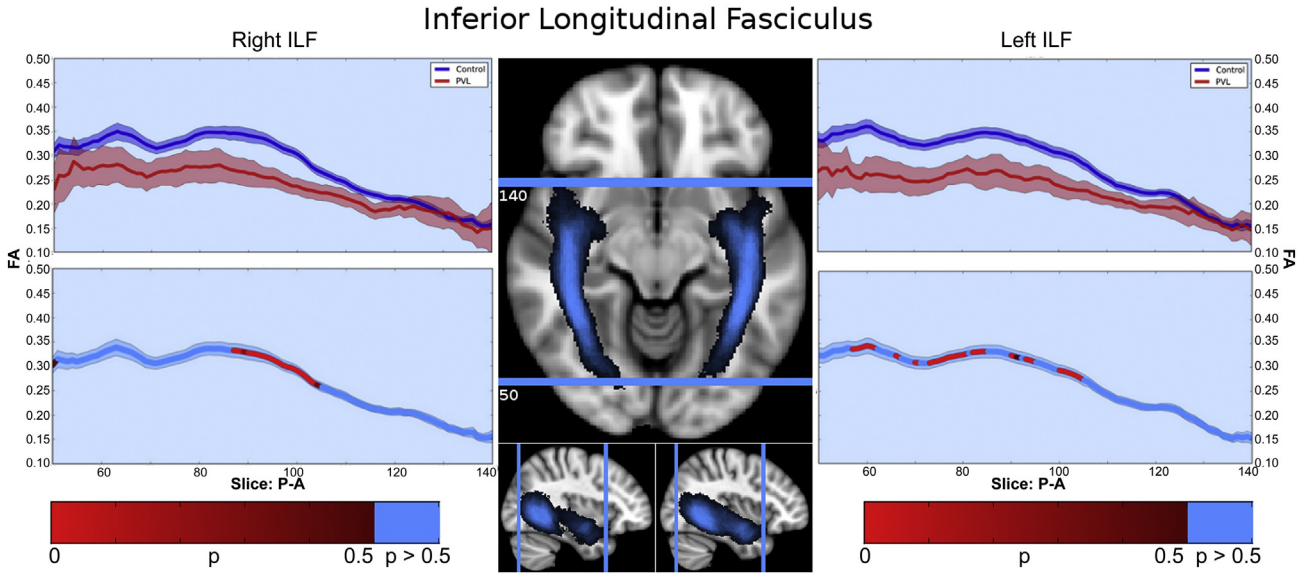

Fig. 4. Inferior longitudinal fasciculus (ILF) along-tract statistics. In the controls, there were two segments identified of the ILF within the fractional anisotropy tract profile which corresponded to the trajectory of the fiber tract extending from the occipital lobe to the temporal lobe. The more posterior occipital segment demonstrated overall higher levels of fractional anisotropy compared to the more anterior temporal lobe segment. No distinct "peaks" were detected. When comparing this FA tract profiles to the preterm PVL cases, the greatest reduction in FA occurred in posterior occipital segment of the tract.

cases, demonstrating no evidence of lateralization. The probabilistic spatial distribution maps did confirm both the anatomic and pathological regional variations (described above) of the ILF in both the controls and preterm PVL cases (Supplementary Fig. 2).

3.4.3. Posterior thalamic radiations

In the controls, there were three segments identified of the PTR within the fractional anisotropy tract profile (Fig. 5) which corresponded to the trajectory of the fiber tract extending from the posterior portion of the thalamus (pulvinar) to the parietal cortex. The more inferior segment demonstrated gradual increasing of fractional anisotropy level up to a "peak", the middle segment corresponding to a drop in fractional anisotropy at the level of the parietal lobe crossing fibers and the third superior parietal segment demonstrated a second peak with gradual decreasing levels of fractional anisotropy noted as the fiber tract extended into the parietal cortical gray matter. When comparing this FA tract profiles to the preterm PVL cases, the greatest reduction in FA occurred in superior parietal segment of the tract. The right and left PTR did show similar distribution of both normal FA variance along the tract in the controls and the pattern of regional FA reduction in the preterm PVL cases, demonstrating no evidence of lateralization. The probabilistic spatial distribution maps did confirm both the anatomic and pathological regional variations (described above) of the PTR in both the controls and preterm PVL cases (Supplementary Fig. 3).

3.4.4. Anterior thalamic radiations

In the controls, there were two main segments observed in the ATR within the fractional anisotropy tract profile (Fig. 6). The first major segment consists of the initially lower FA starting within the thalamus, with a peak centered on the anterior limb of the internal capsule. This more posterior section retains its relative shape when comparing the PVL population to the controls. The second major segment consists of undulating peaks anteriorly, likely a result of densely crossing fibers including the uncinated fasciculus and curving genu of the corpus callosum. The PVL subjects show greater difference between the control subjects in this segment, missing the distinct valleys observed in the regions of crossing fibers. Both right and left ATRs show this pattern, and are reflected in the probabilistic spatial distribution maps (Supplementary Fig. 4).

3.4.5. Superior longitudinal fasciculus (SLF)

In the controls, there were two segments identified of the SLF within the fractional anisotropy tract profile (Fig. 7) which corresponded to the trajectory of the fiber tract extending from the parietal region to the posterior frontal region. The more posterior parietal segment demonstrated gradual increasing of fractional anisotropy level from the parietal cortex to central portion of the tract. The more anterior frontal lobe segment demonstrates gradual decreasing of fractional anisotropy levels from the central portion of the tract to the posterior frontal lobe cortex. There were no distinct peaks noted. When comparing this FA tract profiles to the preterm PVL cases, the greatest reduction in FA occurred in posterior parietal segment of the tract. The right and left did show similar distribution of both normal FA variance along the tract in the controls, but differences in the pattern of regional FA reduction in the preterm PVL cases, with the left sided SLF showing a greater difference in the posterior segment relative to the right side. The probabilistic spatial distribution maps did confirm both the anatomic and pathological regional variations (described above) of the SLF in both the controls and preterm PVL cases (Supplementary Fig. 5).

3.4.6. Optic radiation

In the controls, there were three segments identified of the optic radiations within the fractional anisotropy tract profile (Fig. 8) which corresponded to the trajectory of the fiber tract extending from the lateral geniculate nucleus to the areas of Myer's loop (Segment 1), coursing through the anterior occipital lobe (Segment 2), towards occipital cortex (Segmental 3). The highest peak of FA values was in the posterior occipital segment and the lowest FA values was in the region adjacent to the thalamus (lateral geniculate). When comparing this FA tract profiles to the preterm PVL cases, the greatest reduction in FA occurred in last segment, with a greater reduction noted within the posterior occipital portion of the tract compared to the more anterior segments. The right and left optic radiation did show similar distribution of both normal FA variance along the tract in the controls and the pattern of regional FA reduction in the preterm PVL cases, demonstrating no evidence of lateralization. The probabilistic spatial distribution maps did confirm both the anatomic and pathological regional variations (described above) of the optic radiations in both the controls and preterm PVL cases (Supplementary Fig. 4).

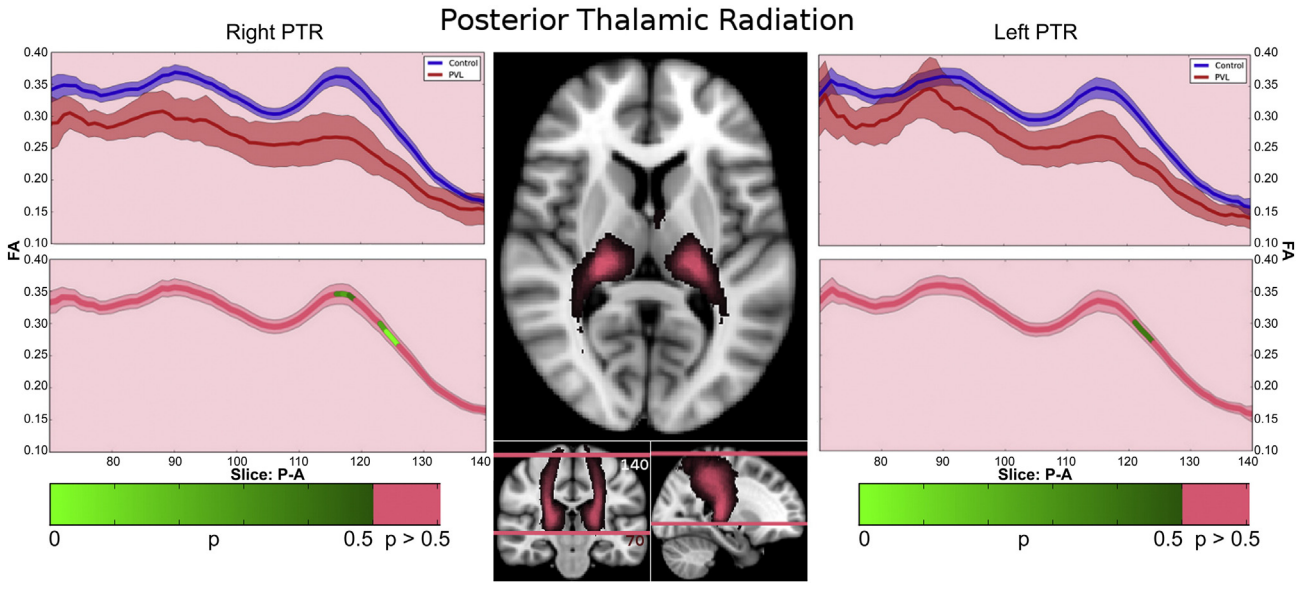

Fig. 5. Posterior thalamic radiation (PTR) along-tract statistics. In the controls, there were three segments identified of the ILF within the fractional anisotropy tract profile which corresponded to the trajectory of the fiber tract extending from the posterior portion of the thalamus (pulvinar) to the parietal cortex. The more inferior segment demonstrated gradual increasing of fractional anisotropy level up to a "peak", the middle segment corresponding to a drop in fractional anisotropy at the level of the parietal lobe crossing fibers and the third superior parietal segment demonstrated a second peak with gradual decreasing levels of fractional anisotropy noted as the fiber tract extended to the parietal cortical gray matter. When comparing this FA tract profiles to the preterm PVL cases, the greatest reduction in FA occurred in superior parietal segment of the tract.

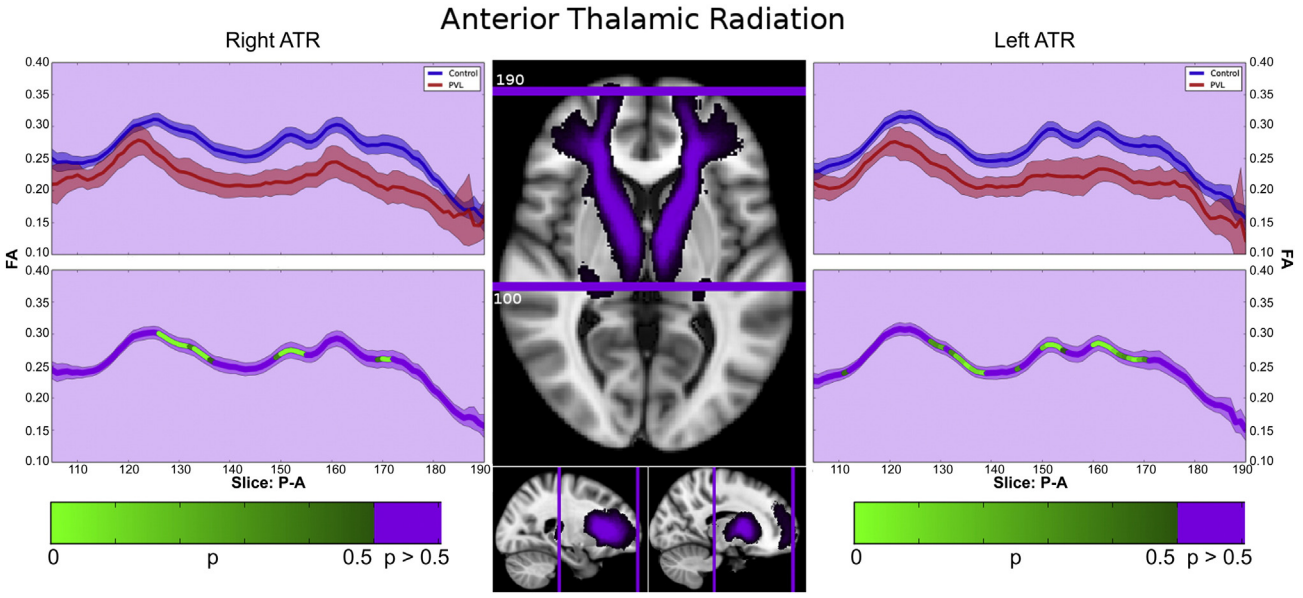

Fig. 6. Anterior thalamic radiations (ATR). In the controls, there were two main segments observed in the ATR within the fractional anisotropy tract profile. The first major segment consists of the initially lower FA starting within the thalamus, with a peak centered on the anterior limb of the internal capsule. This more posterior section retains its relative shape when comparing the PVL population to the controls. The second major segment consists of undulating peaks anteriorly, likely a result of densely crossing fibers including the uncinated fasciculus and curving genu of the corpus callosum. The PVL subjects show greater difference between the control subjects in this segment, missing the distinct valleys observed in the regions of crossing fibers. Both right and left ATRs show this pattern.

3.5. Network topological difference between preterm cerebral palsy and term healthy control subjects

Comparisons between the preterm cerebral palsy patient and control subjects demonstrated that structural white matter network topology in the preterm cerebral palsy patients was altered globally. Specifically, cost and global efficiency were reduced; however, there was no different in assortativity and modularity between the preterm cohort and the term controls.

To better understand the basis of these topological differences, we visualized the network topology of the preterm cerebral palsy group and the controls with regard to community structure (Fig. 9) and then to small-world architecture (Fig. 10). Utilizing the spring-loaded technique, which maps the nodes of a network in accordance with their connection strength rather than anatomical proximity, Fig. 9 demonstrated that, in the preterm cerebral palsy cohort, the global network topology was clustered into four separate modules or subnetworks similar to the term controls (right/left interhemispheric and anterior/posterior

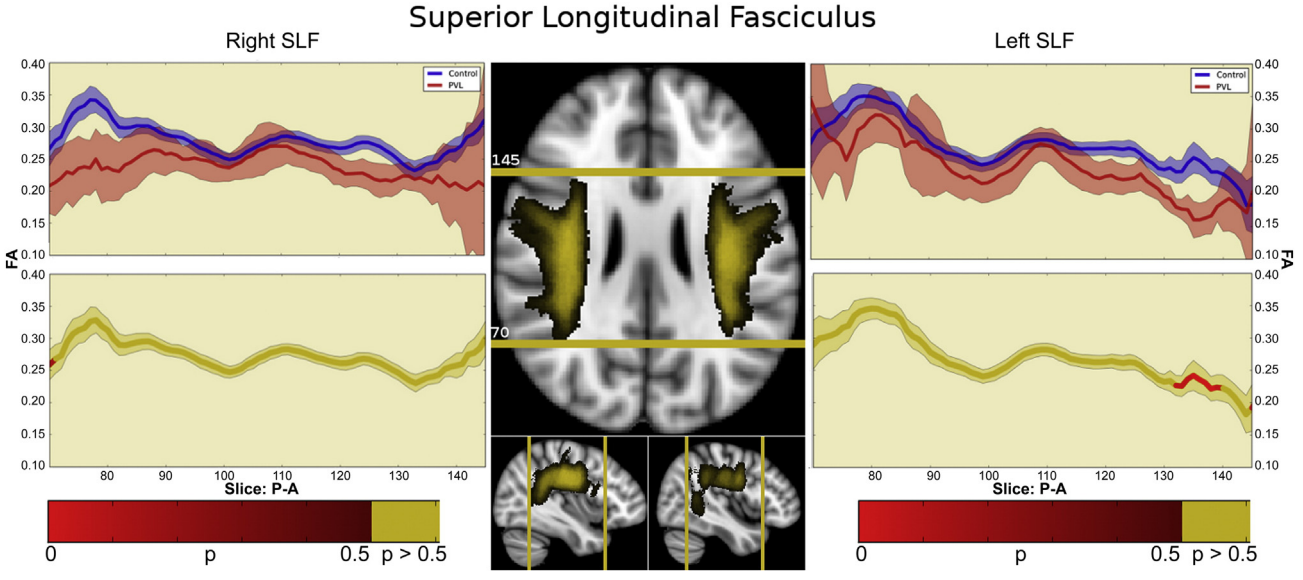

Fig. 7. Superior longitudinal fasciculus (SLF). In the controls, there were two segments identified of the SLF within the fractional anisotropy tract profile which corresponded to the trajectory of the fiber tract extending from the parietal region to the posterior frontal region. The more posterior parietal segment demonstrated gradual increasing of fractional anisotropy level from the parietal cortex to central portion of the tract. The more anterior frontal lobe segment demonstrates gradual decreasing of fractional anisotropy levels from the central portion of the tract to the posterior frontal lobe cortex. There were no distinct peaks noted. When comparing this FA tract profiles to the preterm PVL cases, the greatest reduction in FA occurred in posterior parietal segment of the tract. The right and left did show similar distribution of both normal FA variance along the tract in the controls, but differences in the pattern of regional FA reduction in the preterm PVL cases, with the left sided SLF showing a greater difference in the posterior segment relative to the right side.

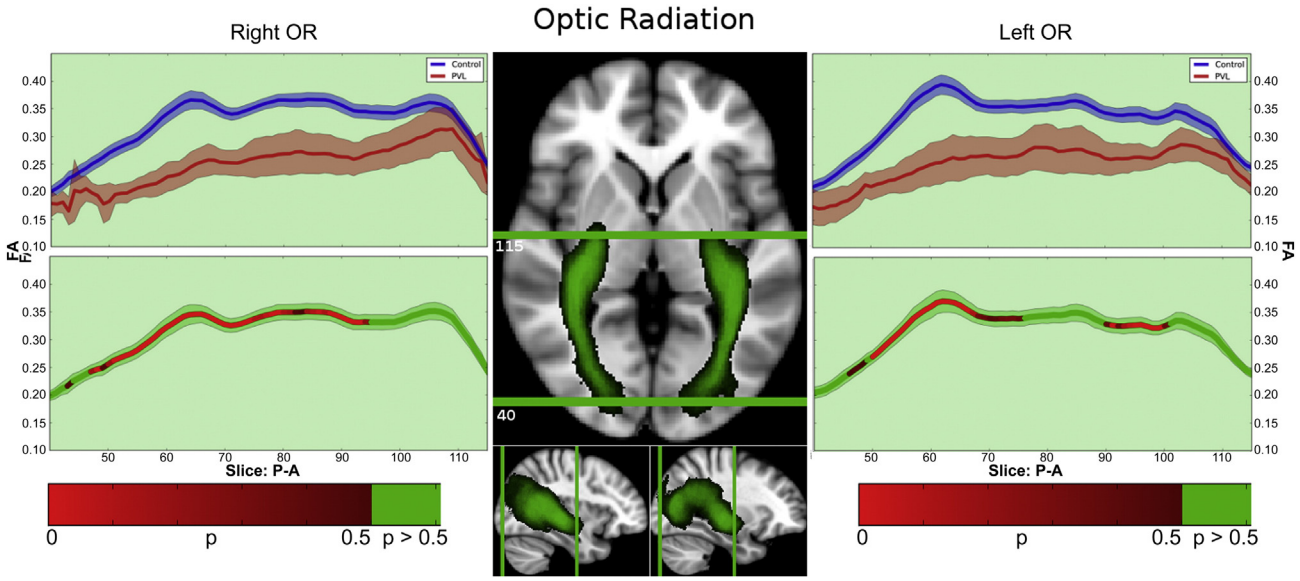

Fig. 8. Optic radiations (OR). In the controls, there were three segmental identified of the optic radiations within the fractional anisotropy tract profile which corresponded to the trajectory of the fiber tract extending from the lateral geniculate region to the areas of Myer's loop (Segment 1), coursing through the anterior occipital lobe (Segment 2), and towards occipital cortex (Segmental 3). The highest peak of FA values was in the posterior occipital segment and the lowest FA values was in the region adjacent to the thalamus (lateral geniculate). When comparing this FA tract profiles to the preterm PVL cases, the greatest reduction in FA occurred in last segment, with a greater reduction noted within the posterior occipital portion of the tract compared to the more anterior segments.

medial interhemispheric). We noted that while the overall number of modules was similar between preterm and term cohort, there were alterations in the anterior aspect of bilateral intrahemispheric modules relative to clusters of frontal, temporal and subcortical (striatal) nodes with regard to the spatial distribution of the intrahemispheric modules related to the medial interhemispheric regions.

Similarly, in Fig. 10, visualization of the small-world architecture using a circle diagram demonstrated a tendency towards less short-range connections (i.e., smaller "arcs", suggesting localized processing) in the frontal, temporal and subcortical regions as well as differences in the number and spatial localization of long-range connections in the frontal, temporal and subcortical regions (i.e., with long-range connections appearing more numerous and clustered in the preterm cerebral palsy cohort rather than uniformly distributed as in the term control cohort) in the frontal, temporal and subcortical regional compared to the parietal–occipital region.

With regard to nodal level alterations, there were multiple parietal-occipital nodes that demonstrated reduced nodal efficiency, local efficiency, and clustering co-efficient ($p < 0.0001$), in the preterm cerebral palsy cohort compared to the term control cohort, corresponding to the regional vulnerability delineated in the along tract analysis (Fig. 11), with relative sparing of the frontal, temporal and subcortical regions. In contrast, there were multiple nodes in the frontal, temporal and subcortical (striatal) regions that demonstrates increased degree, increased local efficiency and increased eigenvector centrality ($p < 0.0001$) in the preterm cerebral palsy cohort compared to the term cohort relative to the parietal–occipital regions (Fig. 12).

3.6. Correlation between along tract and structural network topology measurement and motor and visual clinical outcome scores in preterm cerebral palsy group.

Using principal component analysis, we found that the along tract measurements of the cortical spinal tract and optic radiation demonstrate strong predictive ROC values for both motor (AUC = 0.896) and visual scores (AUC = 0.993) (Fig. 13). With respect to structural network topology measurements, there was a stronger correlation between visual outcomes scores and the global efficiency (−.769) compared to the correlation between global efficiency and motor outcome scores (−.328).

4. Discussion

The major finding of this study is the demonstration of regional vulnerability of posterior aspects of cortical association tracts in preterm children with cerebral palsy corresponding to reorganization of frontal–striatal and frontal–limbic pathways. We have delineated this relationship by combining two innovative analyses: along tract analysis of longitudinal cortical association pathways and structural network topology analyses. We delineated two distinct patterns of regional vulnerability and reorganization, namely: (1) posterior vulnerability of visual-related white matter tracts including the optic radiations and the ventral visual stream correlates of the ILF and the IFOF, as well as the optic radiations and the posterior thalamic radiations corresponding to reduced areas of nodal efficiency in the parietal–occipital regions; and (2) relative preservation of anterior aspects of cortical association tracts that correspond to increased nodal graph structural network topology frontal-striatal and frontal. Both the average tract values and the voxel based TBSS analysis did reveal diffuse microstructural abnormalities in this cohort, but were unable to reveal regional tract alteration of visual cortical association fiber tracts in contrast to the spatial distribution map and along tract analysis.

5. Parietal occipital network vulnerability and preterm cognitive visual dysfunction

Visual impairment is a common sequela of preterm birth and white matter injury and can be due to peripheral problems (retina/optic nerve) and also widespread involvement of the visual pathways at different neuroanatomic levels (cortical or subcortical). Cortical visual impairment (CVI) and cortical visual dysfunction (CVD) clinical profiles can be very heterogeneous and reflect not only the degree of involvement of the visual pathways (including ocular, oculomotor, perceptual and cognitive components) but also be related to neuroplasticity and genetic–environmental influence during maturation. Early recognition

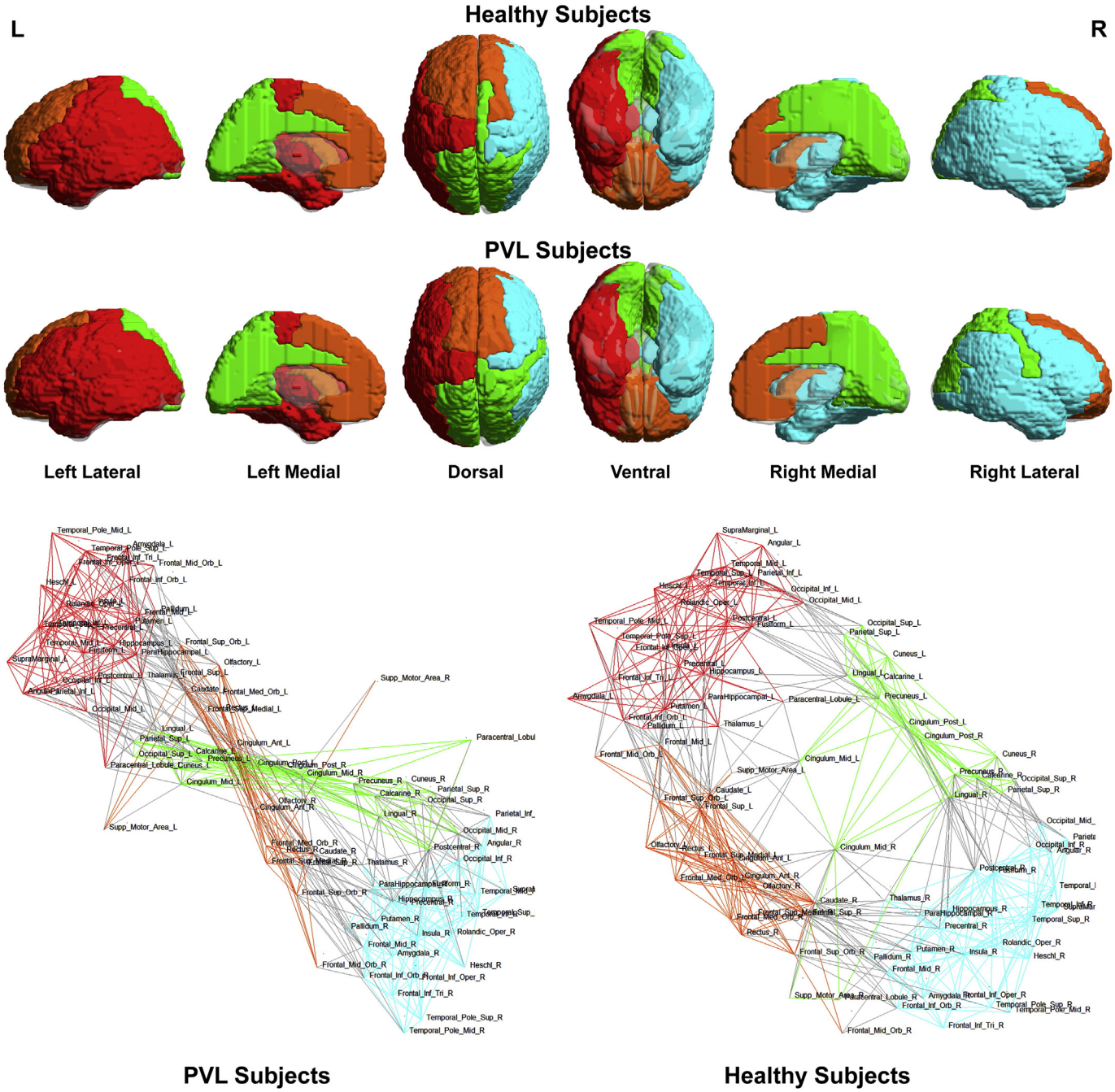

Fig. 9. Spring load topology maps. Spring load maps depict the nodes of a network in accordance with their connection strength rather than anatomical proximity. In the preterm cerebral palsy cohort, the global network topology was clustered into four separate modules or subnetworks similar to the term controls (right/left interhemispheric and anterior/posterior medial interhemispheric). While the overall number of modules was similar between preterm and term cohort, there were alterations in the anterior aspect of bilateral intrahemispheric modules relative to clusters of frontal, temporal and subcortical (striatal) nodes with regard to the spatial distribution of the intrahemispheric modules related to the medial interhemispheric regions.

of CVI/CVD as a cause of visual impairment in preterm children as early as possible does allow for intervention and rehabilitation.

There is literature spanning the last three decades that shows that preterm children who have PVL have impairment of visual–spatial and visual motor integration (Delano-Wood et al., 2009; Ricci et al., 2006; Fazzi et al., 2004; Uggetti et al., 1996; Cioni et al., 1997; Jacobson et al., 1996). More recent work has sought to characterize this visual impairment from within the framework of ventral and dorsal visual pathways for perception and action developed by Goodale and Milner (1992). This framework dichotomizes visual processing into two parallel "streams": the dorsal stream, responsible for visually guided behavior and spatial location, and the ventral stream, responsible for object recognition and representation. In the 1990s, Fedrizzi et al. demonstrated the correlation between MR findings of PVL (ventricular dilations, posterior corpus callosum thinning, optic radiation involvement) and visual perceptual and visual constructive abilities in preterm children with spatic diplegia (Fedrizzi et al., 1996). Fazzi et al. have demonstrated an impairment in the ocular motor coordination task and occipital parietal white matter reduction. Atkinson and Braddock have shown that 6–7 year old preterm children have "dorsal" stream vulnerability with attention deficits that correlated with MRI findings. Furthermore, deficits in ventral visual stream and dorsal stream processing have also been recently detected in preterm children who have PVL and cerebral palsy (Fazzi et al., 2004, 2007). These studies suggest that CVD in preterm children is

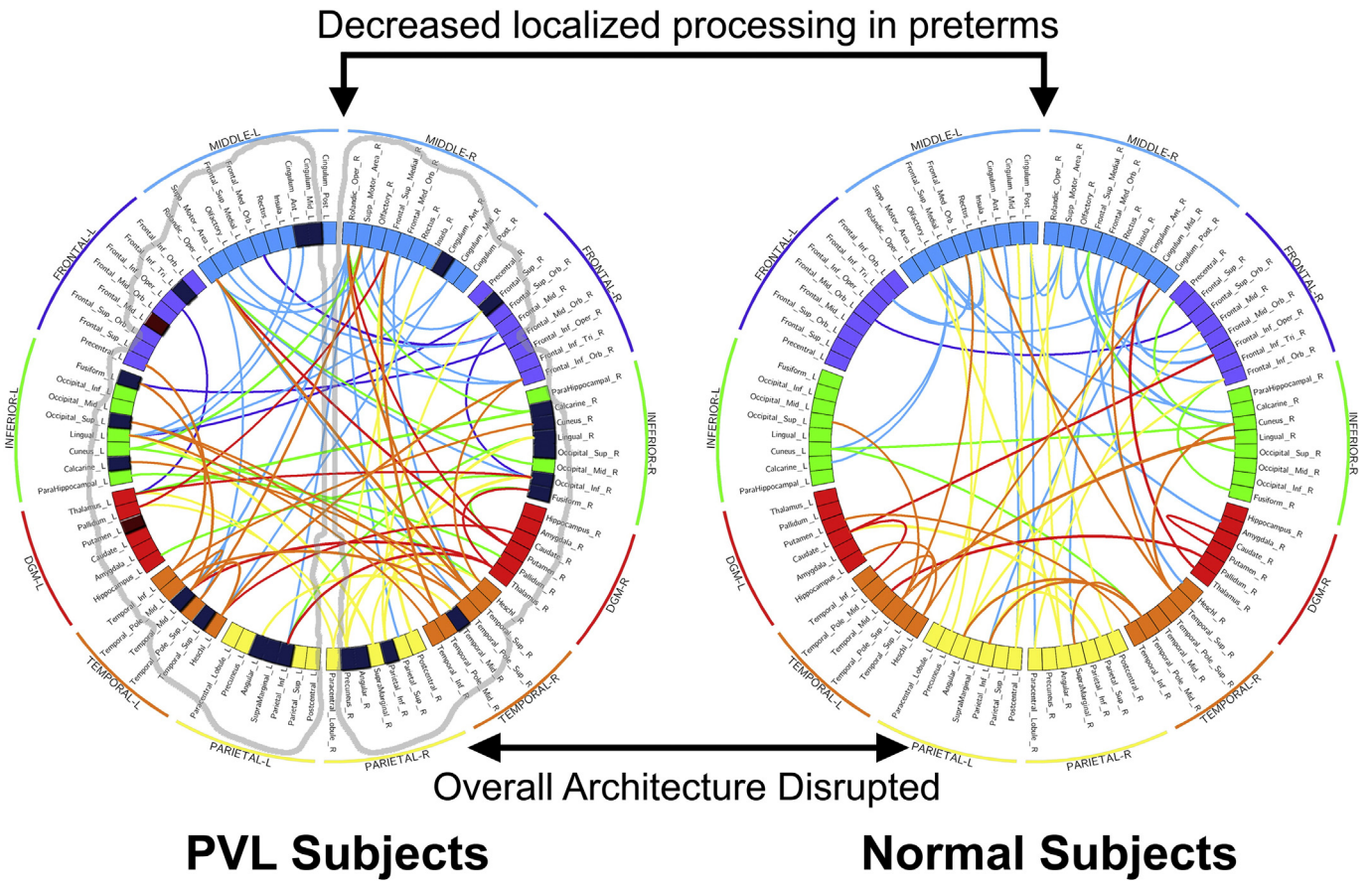

Fig. 10. Small-world architecture. Visualization of the small-world architecture using a circle diagram demonstrated a tendency towards less short-range connections (i.e., smaller "arcs", suggesting localized processing) in the frontal, temporal and subcortical regions as well as differences in the number and spatial localization of long-range connections in the frontal, temporal and subcortical regions (i.e., with long-range connections appearing more numerous and clustered in the preterm cerebral palsy cohort rather than uniformly distributed as in the term control cohort) in the frontal, temporal and subcortical regional compared to the parietal–occipital region.

characterized by both visual spatial dysfunction, and a deficit in object recognition. However, the anatomic substrate for this characterization of CVD has not yet been revealed. Fazzi et al. hypothesized that visual cognitive impairment in the preterm is likely dependent on atypical processing of information in a widespread network of brain region. Additionally, Hoon et al. suggests that the suite of functional disabilities observed in children with CP is better attributed to the interaction between multiple abnormal areas, both gray and white matter, rather than localized effects. Our results support this hypothesis and suggest that an altered occipital–parietal network of disordered connectivity in both the ventral and dorsal visual stream pathways likely underlies cognitive visual dysfunction in preterm children.

There have been multiple studies that have demonstrated that preterm children with varying degrees of gestational age and white matter injury develop different degrees of cerebral visual impairment. CVI is related to retrogeniculate pathways that involve the optic radiations, the occipital cortex, and visual associative areas. There has been much prior work aimed at correlating visual function and the microstructure of optic radiations in preterm neonates. Abnormalities of occipital cortex have also been associated with visual dysfunction in preterm neonates. There is a paucity of structural abnormalities of visual associated areas in preterm neonates including both dorsal and ventral stream regions.

In healthy normally developing preterm neonates, dorsal stream vulnerability can still be detected, as shown in the study by Santos et al. In this study, a group of early gestational age preterm children (25–32 weeks gestation) which were healthy, had no neurological disability, normal IQ or intellect and had normal MRI scans were tested with matched controls for both visual constructive (dorsal) and visual perception test (ventral). The preterm children showed no difference compared to controls in the visual perception test, but did show differences in visual constructive test — evidence that dorsal stream vulnerability is present even in early preterm children without PVL. This study shows that the "dorsal stream vulnerability" that has been hypothesized in multiple neurodevelopment disorders is likely applicable to typically developing preterm children. Santos et al. also found in a healthy preterm group that there were differences in performance of global and configural perceptual processing, showing abnormalities in configural perceptional processing compared to global processing which may also be related to dorsal stream dysfunction compared to visual stream abnormality (Santos et al., 2009, 2010). This is further supported by Atkinson and Birtles et al., who show that preterm children have deficits in networks involving dorsal stream and its connections to parietal frontal and hippocampal areas, using both visual and visual cognitive function test batteries. This supports the theory that lower level dorsal stream deficits in processing of motion and directionality co-exist with higher level perceptual and cognitive processing deficits (Birtles et al., 2007).

5.1. Vulnerability of cortical thalamic, intrahemispheric and interhemispheric connectivity in preterm brain injury

The regional vulnerability/injury pattern could also be related to timing of injury during the preterm period and the peak growth period for the specific cortical association pathway. Both cortical thalamic and interhemispheric pathways are first at risk in early to mid, and then cortical–cortical intrahemispheric connections are at risk in the later preterm period. In this group, the greatest tract difference between

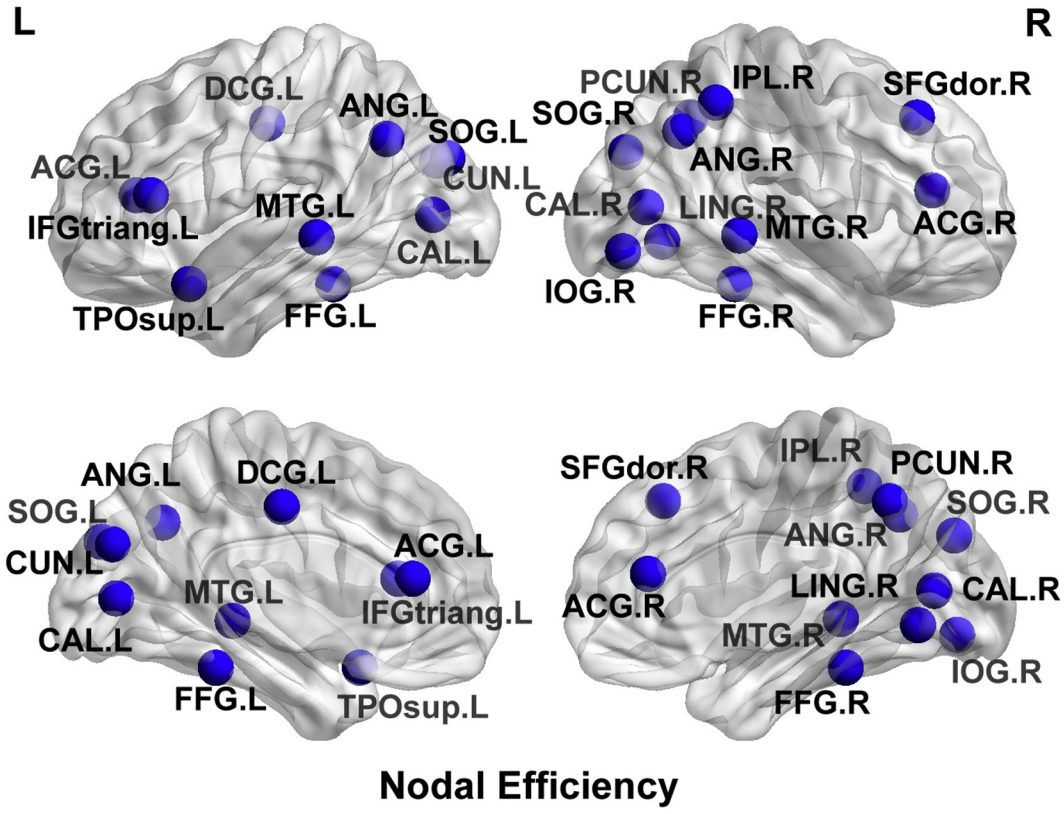

Fig. 11. Nodal efficiency map. 3D glass brain representation showing reduced nodal efficiency in the preterm cerebral palsy cohort compared to the term control cohort, corresponding to the regional vulnerability delineated in the along tract analysis. There is relative sparing of the frontal, temporal and subcortical regions.

preterm and controls was in the splenium of the corpus callosum in the average tract data. However, the degree of abnormality of cortical–thalamic and long range cortical–cortical association fibers was about the same in the average tract data. The regional vulnerability, however, was seen in a greater degree in the cortical thalamic tracts like the optic radiation and posterior thalamic radiations compared to long cortical–cortical association tracts like the SLF and IFOF. This vulnerability is better observed and supported by the regional along tract analysis and spatial distribution maps, whereas the voxel-based and average tract metrics lacked the sensitivity to detect regional variance, mainly due

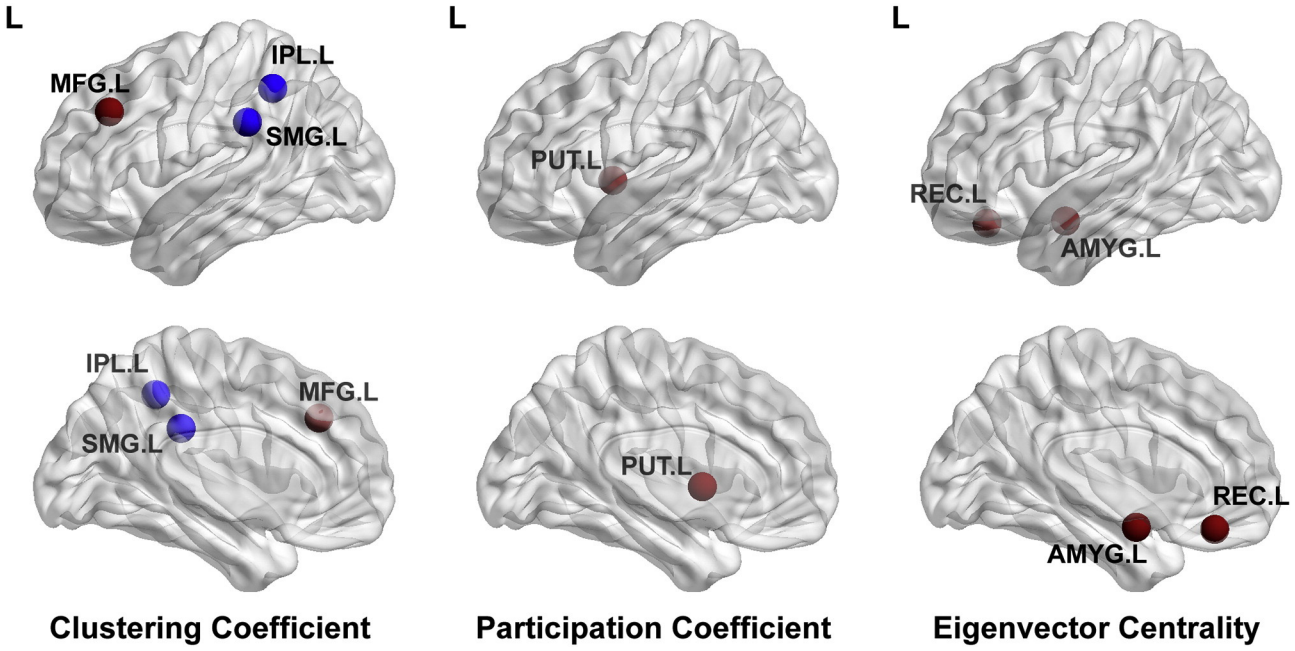

Fig. 12. Nodal level map. 3D glass brain representation coming clustering coefficient, participation coefficient, and eigenvector centrality metrics between control and PVL groups. There were multiple nodes in the frontal, temporal and subcortical (striatal) regions that demonstrates increased degree, increased local efficiency and increased eigenvector centrality ($p < 0.0001$) in the preterm cerebral palsy cohort compared to the term cohort relative to the parietal–occipital regions.

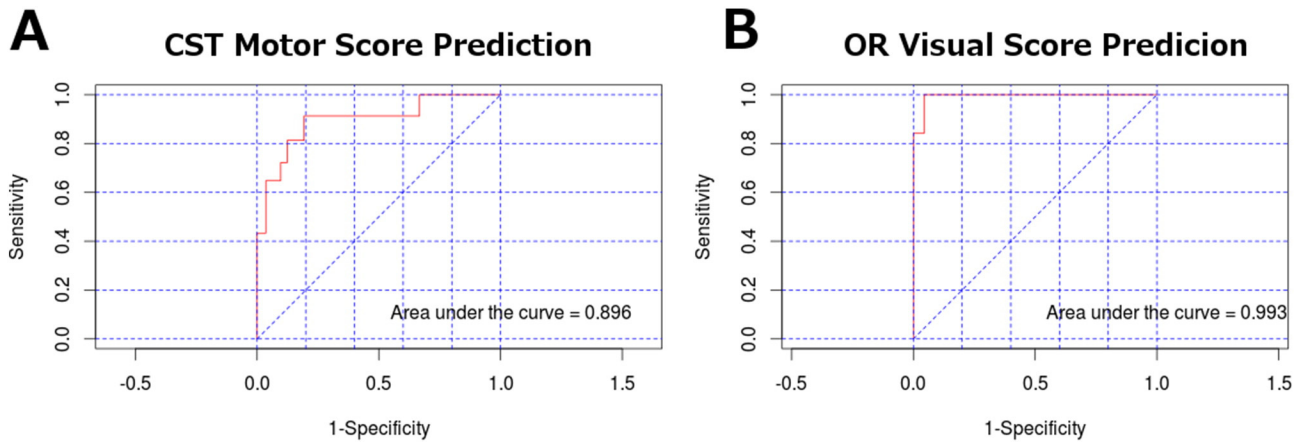

Fig. 13. Predictive power of principal component analysis using area under the ROC (AUROC). A) The set of principal components accounting for 80% of the explained variance in the corticospinal tract were used to predict motor deficiency scores with high predictive power. B) The set of principal components accounting for 80% of the explained variance in the optic radiations were used to predict visual deficit scores with high predictive power.

to the larger global decrease in overall diffusivity observed in the PVL group.

5.2. Relationship to topography and neuropathology of PVL

Preterm infants are highly vulnerable to brain injury resulting in a cognitive disability in multiple domains (Volpe, 2009a), but the neuroanatomic substrate of the cognitive impairments is not completely understood (Ligam et al., 2009; Volpe, 2009b; Kinney, 2009). A major neuropathological finding in preterm infants is periventricular leukomalacia (PVL), a disorder of immature cerebral white matter characterized by focal periventricular necrosis and diffuse gliosis in the surrounding white matter (Ligam et al., 2009; Leviton and Gilles, 1984). Emerging neuropathologic and neuroimaging studies indicate that PVL does not occur in isolation, but rather, is associated with injury to gray matter sites, including the thalamus, cerebral cortex, hippocampus, basal ganglia, cerebellum, and brainstem in variable combinations (Volpe, 2009a; Ligam et al., 2009). This spectrum of gray and white matter injury is now referred to as the "encephalopathy of prematurity" (Ligam et al., 2009; Volpe, 2009b)".

Indeed, the associated damage to certain gray matter regions that are critical to higher cognitive processing may account for the intellectual deficits in preterm survivors with PVL. Of the gray matter structures involved in the encephalopathy of prematurity, the thalamus is critically involved in cognition via extensive interconnections with the cerebral cortex. A recent neuropathologic study of the thalamus in PVL indicates that damage to this structure is present in the majority (59%) of autopsied cases (Ligam et al., 2009). The incidence of such injury in published neuroimaging studies in living children is lower (Ricci et al., 2006; Yokochi, 1997; Giménez et al., 2006; Boardman et al., 2006; Lin et al., 2001; Nosarti et al., 2008) likely reflecting variability in living versus autopsied cohorts and/or incomplete sensitivity of the neuroimaging techniques to detect subtle neuronal loss and/or gliosis observed in histological sections. Magnetic resonance imaging (MRI) studies indicate a diminished volume of thalamus in PVL (Inder et al., 2005a; Inder et al., 2005b; Woodward et al., 2006; Thompson et al., 2007), consistent with atrophy due to diffuse neuronal loss and gliosis detected by neuropathologic examination (Ligam et al., 2009; Pierson et al., 2007). Importantly, decreased thalamic volume in association with PVL correlates with cognitive deficits in survivors (Nosarti et al., 2008; Woodward et al., 2006; Thompson et al., 2007).

Along this vein, we have previously tested the hypothesis that the thalamus is atrophic (reduced in volume) in childhood survivors of prematurity with PVL (diagnosed by conventional MRI), and that the atrophy is associated with microstructural abnormalities within its subdivisions (Nagasunder et al., 2011). We measured diffusivity DTI metrics within the thalamic parenchyma, thereby inferring information about its intrinsic cellular pathology. We sought to determine in particular if there is targeted involvement of microstructural abnormalities in the posterior subdivision of the thalamus (pulvinar) as a potential reflection of the preferential involvement of the posterior (parieto-occipital) white matter in PVL. Interestingly, in this same dataset, we now show posterior vulnerability of visual association fiber tracts including the ILF and the IFOF, as well as abnormal splenium and optic radiations. Other studies have specifically investigated tractography based diffusivity metrics in pediatric populations with CP in order to identify potential biomarkers for predicting clinical outcome. Englander et al. (2013) similarly observed global decrease in diffusivity, along with a significant reduction in diffusivity in long-range connections. Structural connectivity has also been shown to be a potentially useful biomarker in predicting functional improvement after targeted therapy (Englander et al., 2015). Our along-tract methods further expand this, allowing us to observe regional variance along the entire length of the delineated tract, rather than averaging its entire diffusivity profile into one metric. Furthermore, by using a probabilistic tractography algorithm rather than FACT based tracking, we are able to more accurately delineate tracts through regions of crossing fibers. More importantly, probabilistic tractography is better able to continually tract fibers through regions of low FA, which is a particularly important challenge when dealing with a population with global decrease in diffusivity.

This study is limited by the small sample of PVL subjects who had adequate imaging. While we have taken care to sufficiently mitigate the effects of such small sample and high variance, this approach should be tested on a larger cohort. It should also be noted that while the along tract measures were performed using probabilistic tractography, the structural topology analysis instead uses a FACT based algorithm. Using probabilistic tractography to calculate connectivity between every pair of anatomical masks in each subject is computationally prohibitive, and we feel that the delineation necessary for the structural connectivity analysis can be sufficiently approximated using this method. Finally, we are limited in the clinical outcome variables available to us due to the retrospective collection of data. We used the Gross Motor Function Classification System as a measure of motor function severity, which has since been surpassed by more quantitative methods such as the Gross Motor Function Measure 66 (GMFM-66).

6. Conclusion

We have used along-tract analysis and structural network topology analysis to effectively identify not only a selective parietal occipital regional vulnerability but also reorganization of frontal–striatal and frontal–limbic pathways in preterm children with cerebral palsy.

These finding also support the concept that widespread, but selective posterior-anterior neural network connectivity alterations in preterm children with cerebral palsy likely contribute to the pathogenesis of neurosensory and cognitive impairment in this group.

Supplementary data to this article can be found online at http://dx.doi.org/10.1016/j.nicl.2015.08.021.

Acknowledgments

This work was supported by the National Institutes of Health (K23NS063371; P01NS019632), NLM grant 5T15LM007059-27, the Children's Hospital of Pittsburgh Foundation — Harrison Family Fund for Neonatal Neurological Research.

References

Behrens, T.E., Berg, H.J., Jbabdi, S., Rushworth, M.F., Woolrich, M.W., 2007. Probabilistic diffusion tractography with multiple fibre orientations: what can we gain? Neuroimage 34 (1), 144–155. http://dx.doi.org/10.1016/j.neuroimage.2006.09.01817070705.

Birtles, D.B., Braddick, O.J., Wattam-Bell, J., Wilkinson, A.R., Atkinson, J., 2007. Orientation and motion-specific visual cortex responses in infants born preterm. Neuroreport 18 (18), 1975–1979. http://dx.doi.org/10.1097/WNR.0b013e3282f228c818007197.

Boardman, J.P., Counsell, S.J., Rueckert, D., et al., 2006. Abnormal deep grey matter development following preterm birth detected using deformation-based morphometry. Neuroimage 32 (1), 70–78. http://dx.doi.org/10.1016/j.neuroimage.2006.03.02916675269.

Catani, M., Thiebaut de Schotten, M., 2008. A diffusion tensor imaging tractography atlas for virtual in vivo dissections. Cortex 44 (8), 1105–1132. http://dx.doi.org/10.1016/j.cortex.2008.05.00418619589.

Ceschin, R., Wisnowski, J.L., Paquette, L.B., Nelson, M.D., Blüml, S., Panigrahy, A., 2015. Developmental synergy between thalamic structure and interhemispheric connectivity in the visual system of preterm infants. Neuroimage Clin. 8, 462–472. http://dx.doi.org/10.1016/j.nicl.2015.05.01426106571.

Chang, M.C., Jang, S.H., Yoe, S.S., et al., 2012. Diffusion tensor imaging demonstrated radiologic differences between diplegic and quadriplegic cerebral palsy. Neurosci. Lett. 512 (1), 53–58. http://dx.doi.org/10.1016/j.neulet.2012.01.06522330748.

Cioni, G., Fazzi, B., Coluccini, M., Bartalena, L., Boldrini, A., van Hof-van Duin, J., 1997. Cerebral visual impairment in preterm infants with periventricular leukomalacia. Pediatr. Neurol. 17 (4), 331–338. http://dx.doi.org/10.1016/S0887-8994(97)00152-59436798.

Counsell, S.J., Dyet, L.E., Larkman, D.J., et al., 2007. Thalamo-cortical connectivity in children born preterm mapped using probabilistic magnetic resonance tractography. Neuroimage 34 (3), 896–904. http://dx.doi.org/10.1016/j.neuroimage.2006.09.03617174575.

Delano-Wood, L., Bondi, M.W., Sacco, J., et al., 2009. Heterogeneity in mild cognitive impairment: differences in neuropsychological profile and associated white matter lesion pathology. J. Int. Neuropsychol. Soc. 15 (6), 906–914. http://dx.doi.org/10.1017/S1355617709990025719891820.

Englander, Z.A., Pizoli, C.E., Batrachenko, A., et al., 2013. Diffuse reduction of white matter connectivity in cerebral palsy with specific vulnerability of long range fiber tracts. Neuroimage Clin. 2 (1), 440–447. http://dx.doi.org/10.1016/j.nicl.2013.03.00624179798.

Englander, Z.A., Sun, J., Case, L., Mikati, M.A., Kurtzberg, J., Song, A.W., 2015. Brain structural connectivity increases concurrent with functional improvement: evidence from diffusion tensor MRI in children with cerebral palsy during therapy. Neuroimage Clin. 7, 315–324. http://dx.doi.org/10.1016/j.nicl.2015.01.00225610796.

Fazzi, E., Bova, S.M., Uggetti, C., et al., 2004. Visual-perceptual impairment in children with periventricular leukomalacia. Brain Dev. 26 (8), 506–512. http://dx.doi.org/10.1016/j.braindev.2004.02.00215533651.

Fazzi, E., Signorini, S.G., Bova, S.M., et al., 2007. Spectrum of visual disorders in children with cerebral visual impairment. J. Child Neurol. 22 (3), 294–301. http://dx.doi.org/10.1177/08830738070220030080117621499.

Fedrizzi, E., Inverno, M., Bruzzone, M.G., Botteon, G., Saletti, V., Farinotti, M., 1996. MRI features of cerebral lesions and cognitive functions in preterm spastic diplegic children. Pediatr. Neurol. 15 (3), 207–212. http://dx.doi.org/10.1016/S0887-8994(96)00174-98916157.

Fruchterman, T.M.J., Reingold, E.M., 1991. Graph drawing by force-directed placement. Software-Practice Exp 21 (11), 1129–1164.

Gerig, G., Gouttard, S., Corouge, I., 2004. Analysis of brain white matter via fiber tract modeling. Conf Proc IEEE Eng Med Biol Soc 6, 4421–4424. http://dx.doi.org/10.1109/IEMBS.2004.140422917271286.

Giménez, M., Junqué, C., Narberhaus, A., Botet, F., Bargalló, N., Mercader, J.M., 2006. Correlations of thalamic reductions with verbal fluency impairment in those born prematurely. Neuroreport 17 (5), 463–466. http://dx.doi.org/10.1097/01.wnr.0000209008.93846.2416543807.

Goodale, M.A., Milner, A.D., 1992. Separate visual pathways for perception and action. Trends Neurosci. 15 (1), 20–25. http://dx.doi.org/10.1016/0166-2236(92)90344-81374953.

Hoon, A.H., Lawrie, W.T., Melhem, E.R., et al., 2002. Diffusion tensor imaging of periventricular leukomalacia shows affected sensory cortex white matter pathways. Neurol. 59 (5), 752–756. http://dx.doi.org/10.1212/WNL.59.5.75212221171.

Hoon, A.H., Stashinko, E.E., Nagae, L.M., et al., 2009. Sensory and motor deficits in children with cerebral palsy born preterm correlate with diffusion tensor imaging abnormalities in thalamocortical pathways. Dev. Med. Child Neurol. 51 (9), 697–704. http://dx.doi.org/10.1111/j.1469-8749.2009.03306.x19416315.

Inder, T., Neil, J., Yoder, B., Rees, S., 2005a. Patterns of cerebral injury in a primate model of preterm birth and neonatal intensive care. J. Child Neurol. 20 (12), 965–967. http://dx.doi.org/10.1177/08830738050200120601164178 43.

Inder, T.E., Warfield, S.K., Wang, H., Hüppi, P.S., Volpe, J.J., 2005b. Abnormal cerebral structure is present at term in premature infants. Pediatrics 115 (2), 286–294. http://dx.doi.org/10.1542/peds.2004-032615687434.

Jacobson, L., Ek, U., Fernell, E., Flodmark, O., Broberger, U., 1996. Visual impairment in preterm children with periventricular leukomalacia — visual, cognitive and neuropaediatric characteristics related to cerebral imaging. Dev. Med. Child Neurol. 38 (8), 724–735. http://dx.doi.org/10.1111/j.1469-8749.1996.tb12142.x8761168.

Jenkinson, M., Beckmann, C.F., Behrens, T.E., Woolrich, M.W., Smith, S.M., 2012. FSL. Neuroimage 62 (2), 782–790. http://dx.doi.org/10.1016/j.neuroimage.2011.09.01521979382.

Kinney, H.C., 2009. The encephalopathy of prematurity: one pediatric neuropathologist's perspective. Semin. Pediatr. Neurol. 16 (4), 179–190. http://dx.doi.org/10.1016/j.spen.2009.09.00319945652.

Krzywinski, M., Schein, J., Birol, I., et al., 2009. Circos: an information aesthetic for comparative genomics. Genome Res. 19 (9), 1639–1645. http://dx.doi.org/10.1101/gr.092759.10919541911.

Ledberg, A., Fransson, P., Larsson, J., Petersson, K.M., 2001. A 4D approach to the analysis of functional brain images: application to FMRI data. Hum Brain Mapp. 13 (4), 185–198 http://www.ncbi.nlm.nih.gov/pubmed/11410948.

Lee, J.D., Park, H.-J., Park, E.S., et al., 2011. Motor pathway injury in patients with periventricular leucomalacia and spastic diplegia. Brain 134 (4), 1199–1210. http://dx.doi.org/10.1093/brain/awr02121385750.

Leviton, A., Gilles, F.H., 1984. Acquired perinatal leukoencephalopathy. Ann. Neurol. 16 (1), 1–8. http://dx.doi.org/10.1002/ana.4101601026465860.

Ligam, P., Haynes, R.L., Folkerth, R.D., et al., 2009. Thalamic damage in periventricular leukomalacia: novel pathologic observations relevant to cognitive deficits in survivors of prematurity. Pediatr. Res. 65 (5), 524–529. http://dx.doi.org/10.1203/PDR.0b013e3181998baf19127204.

Lin, Y., Okumura, A., Hayakawa, F., Kato, K., Kuno, T., Watanabe, K., 2001. Quantitative evaluation of thalami and basal ganglia in infants with periventricular leukomalacia. Dev. Med. Child Neurol. 43 (7), 481–485. http://dx.doi.org/10.1017/S0012162201000883 11463180.

Ludeman, N.A., Berman, J.I., Wu, Y.W., et al., 2008. Diffusion tensor imaging of the pyramidal tracts in infants with motor dysfunction. Neurol. 71 (21), 1676–1682. http://dx.doi.org/10.1212/01.wnl.0000304084.59964.e218448871.

Mori, S., Zhang, J., 2006. Principles of diffusion tensor imaging and its applications to basic neuroscience research. Neuron 51 (5), 527–539. http://dx.doi.org/10.1016/j.neuron.2006.08.01216950152.

Murakami, A., Morimoto, M., Yamada, K., et al., 2008. Fiber-tracking techniques can predict the degree of neurologic impairment for periventricular leukomalacia. Pediatrics 122 (3), 500–506. http://dx.doi.org/10.1542/peds.2007-281618762518.

Nagae, L.M., Hoon, A.H., Stashinko, E., et al., 2007. Diffusion tensor imaging in children with periventricular leukomalacia: variability of injuries to white matter tracts. A.J.N.R. Am. J. Neuroradiol. 28 (7), 1213–1222. http://dx.doi.org/10.3174/ajnr.A053417698519.

Nagasunder, A.C., Kinney, H.C., Blüml, S., et al., 2011. Abnormal microstructure of the atrophic thalamus in preterm survivors with periventricular leukomalacia. A.J.N.R. Am. J. Neuroradiol. 32 (1), 185–191. http://dx.doi.org/10.3174/ajnr.A224320930003.

Nosarti, C., Giouroukou, E., Healy, E., et al., 2008. Grey and white matter distribution in very preterm adolescents mediates neurodevelopmental outcome. Brain 131 (1), 205–217. http://dx.doi.org/10.1093/brain/awm28218056158.

Palisano, R., Bartlett, D., Livingston, M., 2007. Gross Motor Function Classification System — Expanded and Revised.

Palisano, R., Rosenbaum, P., Walter, S., Russell, D., Wood, E., Galuppi, B., 1997. Development and reliability of a system to classify gross motor function in children with cerebral palsy. Dev. Med. Child Neurol. 39 (4), 214–223. http://dx.doi.org/10.1111/j.1469-8749.1997.tb07414.x9183258.

Pandit, A.S., Robinson, E., Aljabar, P., et al., 2014. Whole-brain mapping of structural connectivity in infants reveals altered connection strength associated with growth and preterm birth. Cereb. Cortex 24 (9), 2324–2333. http://dx.doi.org/10.1093/cercor/bht08623547135.

Panigrahy, A., Barnes, P.D., Robertson, R.L., et al., 2001. Volumetric brain differences in children with periventricular T2-signal hyperintensities: a grouping by gestational age at birth. A.J.R. Am. J. Roentgenol. 177 (3), 695–702. http://dx.doi.org/10.2214/ajr.177.3.177069511517078.

Paquette, L.B., Wisnowski, J.L., Ceschin, R., et al., 2013. Abnormal cerebral microstructure in premature neonates with congenital heart disease. A.J.N.R. Am. J. Neuroradiol. 34 (10), 2026–2033. http://dx.doi.org/10.3174/ajnr.A352823703146.

Pierson, C.R., Folkerth, R.D., Billiards, S.S., et al., 2007. Gray matter injury associated with periventricular leukomalacia in the premature infant. Acta Neuropathol. 114 (6), 619–631. http://dx.doi.org/10.1007/s00401-007-0295-517912538.

Rai, Y., Chaturvedi, S., Paliwal, V.K., et al., 2013. DTI correlates of cognition in term children with spastic diplegic cerebral palsy. Eur. J. Paediatr. Neurol. 17 (3), 294–301. http://dx.doi.org/10.1016/j.ejpn.2012.11.00523246381.

Rha, D.W., Chang, W.H., Kim, J., Sim, E.G., Park, E.S., 2012. Comparing quantitative tractography metrics of motor and sensory pathways in children with periventricular

leukomalacia and different levels of gross motor function. Neuroradiology 54 (6), 615–621. http://dx.doi.org/10.1007/s00234-011-0996-222170081.
Ricci, D., Anker, S., Cowan, F., et al., 2006. Thalamic atrophy in infants with PVL and cerebral visual impairment. Early Hum. Dev. 82 (9), 591–595. http://dx.doi.org/10.1016/j.earlhumdev.2005.12.00716500047.
Rivkin, M.J., Watson, C.G., Scoppettuolo, L.A., et al., 2013. Adolescents with D-transposition of the great arteries repaired in early infancy demonstrate reduced white matter microstructure associated with clinical risk factors. J. Thorac. Cardiovasc. Surg. 146 (3), 543–549.e1. http://dx.doi.org/10.1016/j.jtcvs.2012.12.00623375991.
Rose, J., Mirmiran, M., Butler, E.E., et al., 2007. Neonatal microstructural development of the internal capsule on diffusion tensor imaging correlates with severity of gait and motor deficits. Dev. Med. Child Neurol. 49 (10), 745–750. http://dx.doi.org/10.1111/j.1469-8749.2007.00745.x17880643.
Rose, S., Guzzetta, A., Pannek, K., Boyd, R., 2011. MRI structural connectivity, disruption of primary sensorimotor pathways, and hand function in cerebral palsy. Brain Connect. 1 (4), 309–316. http://dx.doi.org/10.1089/brain.2011.003422432420.
Rubinov, M., Sporns, O., 2010. Complex network measures of brain connectivity: uses and interpretations. Neuroimage 52 (3), 1059–1069. http://dx.doi.org/10.1016/j.neuroimage.2009.10.00319819337.
Santos, A., Duret, M., Mancini, J., Busuttil, M., Deruelle, C., 2010. Does preterm birth affect global and configural processing differently? Dev. Med. Child Neurol. 52 (3), 293–298. http://dx.doi.org/10.1111/j.1469-8749.2009.03398.x19694779.
Santos, A., Duret, M., Mancini, J., Gire, C., Deruelle, C., 2009. Preterm birth affects dorsal-stream functioning even after age 6. Brain Cogn. 69 (3), 490–494. http://dx.doi.org/10.1016/j.bandc.2008.10.00519081169.
Scheck, S.M., Boyd, R.N., Rose, S.E., 2012. New insights into the pathology of white matter tracts in cerebral palsy from diffusion magnetic resonance imaging: a systematic review. Dev. Med. Child Neurol. 54 (8), 684–696. http://dx.doi.org/10.1111/j.1469-8749.2012.04332.x22646844.
Thomas, B., Eyssen, M., Peeters, R., et al., 2005. Quantitative diffusion tensor imaging in cerebral palsy due to periventricular white matter injury. Brain 128 (11), 2562–2577. http://dx.doi.org/10.1093/brain/awh60016049045.
Thompson, D.K., Warfield, S.K., Carlin, J.B., et al., 2007. Perinatal risk factors altering regional brain structure in the preterm infant. Brain 130 (3), 667–677. http://dx.doi.org/10.1093/brain/awl27717008333.
Trivedi, R., Agarwal, S., Shah, V., et al., 2010. Correlation of quantitative sensorimotor tractography with clinical grade of cerebral palsy. Neuroradiology 52 (8), 759–765. http://dx.doi.org/10.1007/s00234-010-0703-820405112.
Tzourio-Mazoyer, N., Landeau, B., Papathanassiou, D., et al., 2002. Automated anatomical labeling of activations in SPM using a macroscopic anatomical parcellation of the MNI MRI single-subject brain. Neuroimage 15 (1), 273–289. http://dx.doi.org/10.1006/nimg.2001.097811771995.
Uggetti, C., Egitto, M.G., Fazzi, E., et al., 1996. Cerebral visual impairment in periventricular leukomalacia: MR correlation. A.J.N.R. Am. J. Neuroradiol. 17 (5), 979–9858733977.
Volpe, J.J., 2009a. Brain injury in premature infants: a complex amalgam of destructive and developmental disturbances. Lancet Neurol. 8 (1), 110–124. http://dx.doi.org/10.1016/S1474-4422(08)70294-119081519.
Volpe, J.J., 2009b. The encephalopathy of prematurity — brain injury and impaired brain development inextricably intertwined. Semin. Pediatr. Neurol. 16 (4), 167–178. http://dx.doi.org/10.1016/j.spen.2009.09.00519945651.
Woodward, L.J., Anderson, P.J., Austin, N.C., Howard, K., Inder, T.E., 2006. Neonatal MRI to predict neurodevelopmental outcomes in preterm infants. N. Engl. J. Med. 355 (7), 685–694. http://dx.doi.org/10.1056/NEJMoa05379216914704.
Yokochi, K., 1997. Thalamic lesions revealed by MR associated with periventricular leukomalacia and clinical profiles of subjects. Acta Paediatr. 86 (5), 493–496. http://dx.doi.org/10.1111/j.1651-2227.1997.tb08919.x9183488.
Yoshida, S., Hayakawa, K., Yamamoto, A., et al., 2010. Quantitative diffusion tensor tractography of the motor and sensory tract in children with cerebral palsy. Dev. Med. Child Neurol. 52 (10), 935–940. http://dx.doi.org/10.1111/j.1469-8749.2010.03669.x20412261.